Dominant wave energy and sediment movement on intertidal beaches in Freshwater Bay, Washington, U.S.A.

Niall Twomey

A report prepared in partial fulfillment of
the requirements for the degree of

Master of Science
Earth and Space Sciences: Applied Geosciences

University of Washington

March 2015

Project mentor:
David Parks
Washington
Department of Natural Resources

Internship coordinator:
Kathy Troost

Reading committee:
Andrea Ogston
Brian Collins

MESSAGe Technical Report Number: 018

Abstract
Freshwater Bay (FWB), Washington did not undergo significant erosion of its shoreline after the construction of the Elwha and Glines Canyon Dams, unlike the shoreline east of Angeles Point (the Elwha River's lobate delta). In this paper I compare the wave energy density in the western and eastern ends of the Strait of Juan de Fuca with the wave energy density at the Elwha River delta. This indicates seasonal high- and low-energy regimes in the energy density data. I group multi-year surveys of four cross-shore transects in FWB along this seasonal divide and search for seasonal trends in profile on the foreshore. After documenting changes in elevation at specific datums on the foreshore, I compare digital images of one datum to determine the particle sizes that are transported during deposition and scour events on this section of the FWB foreshore. Repeat surveys of four cross-shore transects over a five-year period indicate a highly mobile slope break between the upper foreshore and the low-tide delta. Post-2011, profiles in eastern FWB record deposition in the landward portion of the low-tide terrace and also in the upper intertidal. Western FWB experiences transient deposition on the low-tide terrace and high intra-annual variability in beach profile. Profile elevation at the slope break in western FWB can vary 0.5 m in the course of weeks. Changes in surface sediment that range from sand to cobble are co-incident with these changes in elevation. High sediment mobility and profile variation are inconsistent with shoreline stability and decreased sediment from the presumed source on the Elwha River delta.

Table of Contents

List of Figures

List of Tables

Acknowledgements

I would like to thank my wife for her patience and support during what must have seemed like a never-ending degree process. I would also like to thank Dave Parks of Washington Department of Natural Resources and Jon Warrick of United States Geological Survey. Dave supplied the beach profiles and the images of beach sediment in Freshwater Bay and Jon allowed me to use data from a nearshore tripod the USGS deployed in Freshwater Bay. Lastly, I would like to thank Emily Eidam for her help with Matlab questions.

Introduction

Freshwater Bay (FWB) is a coastal embayment on the southern edge of the Strait of Juan de Fuca (SJF). In FWB, cross-shore beach profiles show variation in elevation, topography, and surface grain size on annual, seasonal, and, according to Miller et al. (2011) perhaps even daily scales. In SJF, dominant waves oscillate between low- and high-energy regimes on annual scales. Understanding sediment movement in FWB will provide a better understanding of the littoral system that includes the mouth of the Elwha River and the shoreline east of the delta.

Removal of two dams between 2011-2014 restored delivery of Elwha River sediment to the delta that forms the eastern boundary of FWB (Duda et al., 2011). FWB is west of the Elwha River delta and the city of Port Angeles, Washington. Baseline studies of FWB, the Elwha River delta, and the embayment between the delta and Ediz Hook provide a wealth of information about the area (Warrick et al., 2008; Warrick et al., 2009; Duda et al., 2011; Miller et al., 2011; Warrick et al., 2011). Restoration of a free-flowing Elwha River provides a pulse of sediment to the coast that can be tracked to the east (Gelfenbaum et al., 2015), but an understanding of sediment transport in FWB is necessary to understand the entire littoral cell.

In this paper I present the wave regime recorded at two permanent instrument moorings in the SJF (Fig 1) and at a nearshore instrument tripod in FWB. I then describe changes in beach profile and surface grain size in FWB at four cross-shore transects (Fig 2) from 2010-2014.

The dominant wave regime in the SJF is swell from the Pacific Ocean that breaks on the western face of the Elwha delta (Fig 3). This swell decreases in wave height and wave energy as it travels eastward in SJF (Gelfenbaum et al., 2009; Warrick et al., 2011). Waves both activate and transport sediment on the beach face (Komar, 1976). This movement can be parallel to the shoreline as suspended load in the surf zone, known as longshore transport, or in the swash zone as bedload, known as swash transport (Komar, 1976). It can also be cross-shore sediment transport that is perpendicular to the shoreline (Komar, 1976).

The classic explanation of changes in beach profile is that higher energy and steeper waves predominate in winter and erode sediment from the upper intertidal (Komar, 1976). In contrast, milder summer conditions are traditionally viewed as periods when sediment is transported landward and deposited in the upper intertidal (Komar, 1976).

Due to the interaction between sediment supply and littoral wave energy, the shorelines on each side of the Elwha River delta behave differently (Gelfenbaum et al., 2009). The shoreline east of the Elwha River mouth has been receding for most of the 20th century (Warrick et al., 2009). This recession is attributed to interrupted sediment flow after dam construction (Duda et al., 2011). Increased sediment supply following the removal of the dams resulted in prograding shorelines and fining of sediments on the low-tide terrace east of the delta (Miller, 2014). FWB did not experience comparable erosion or shoreline

regression after dam construction (Duda et al., 2011), but the Elwha River is the only likely major source of sediment for distribution in FWB.

The coastal bluffs of FWB are relatively unstudied, but aerial images indicate frequent small-scale bluff failure in the central portion of FWB. An accumulation of sand at the westernmost end of FWB could not be supplied by these bluff failures, though they would add to the sediment budget in the central and eastern portions of FWB. The only other potential sources of sediment for FWB are the beaches farther west. Since these beaches are separated from FWB by 6.5 km of rocky bluff and by bathymetry that drops quickly offshore, it is unlikely that they contribute appreciable sediment to FWB.

During a site visit in January 2015, I observed evidence of predominantly eastward transport along the western portion of FWB at both Mean High Water and at the slope break. This evidence consisted of tree trunks with root balls to the west and their tops pointing east, accretion on the west side and scour on the east side of logs and rocks, spits of gravel and sand extending eastward from shore-parallel logs and across the mouth of Coville Creek, and finally a drift of sand across the boat ramp in western FWB at the elevation of the SB. Evidence of cross-shore transport, in the form of cusps and embayments, is readily identifiable in the eastern portion of FWB.

This study is a description of changes that occurred on four transects in Freshwater Bay from 2010-2014. I compare the wave regime recorded at two permanent instrument moorings in the SJF with the wave regime at a nearshore instrument tripod. Profiles of the beach slope that extend from above Mean High Water (MHW) to below Mean Low Water (MLW) will be used to show that material accretion and loss are not strictly seasonal, but are highly active throughout the year. FWB then, has a highly active intertidal zone, major sediment source in the area to the east, a bedrock outcrop to the west, and wave energy delivered from the west.

Scope of work

First, I show the frequency and direction of dominant period waves at each instrument location (Fig 3). I use the wave height to derive and plot wave energy density. I also show that wave energy density is different at each buoy location (Fig 4). I use the wave energy density data to divide the wave regime into high- and low-energy components based on a notable summer-time decrease in the energy density maximum values (Fig 4).

Second, I use the location of Mean High Water (MHW), Mean Sea Level (MSL), Mean Low Water (MLW), and the Slope Break (SB) on transect profiles to show that changes in the beach elevation can happen in a relatively short period of time. These changes do not appear to be seasonal, or strictly based on the high- and low-energy division that I have made. I also use the profiles in a Eulerian representation of a control volume. Viewed through time this shows the locations of MHW, MSL, MLW, and SB advancing seaward as sediment is deposited or regressing shoreward as it is scoured away.

Third, I categorize digital images of the surface sediment into four groups: cobble, gravel, sand, and sand-with-fines. Correlating sediment gain/loss with the change in surface sediment size broadly indicates the grain size being transported. I originally used an autocorrelation program to estimate the mean grain size of each digital image. Due to environmental conditions outside the parameters required for the autocorrelation process and the bi-modal distribution of some images, I substituted the four-category characterization of sediment size.

There are limitations unique to each of the three wave datasets. The NOAA (National Oceanic and Atmospheric Administration) 3-meter discus buoy at Neah Bay has considerable periods with no data collected, the longest of these is five months, and there is no data at all for 2010. The NOAA buoy at New Dungeness has the most complete record, but does have occasional data gaps of 2-3 weeks. The USGS (United States Geological Survey) Freshwater Bay near-bed dataset only contains data from December 2010 to September 2011. Also, this dataset was recorded less frequently than the NOAA buoys.

Sampling frequency for the beach profiles is less than the scale of morphologic variation on the foreshore of Freshwater Bay. Finer resolution of sediment transport can therefore be missed within this data set.

Background

Geologic setting

Freshwater Bay is an arcuate shoreline midway along the southern edge of the Strait of Juan de Fuca and west of the Elwha River delta. Observatory Point is its western terminus and the cuspate deposit of the Elwha River delta forms its eastern edge.

During the Fraser Glaciation, the Juan de Fuca lobe of the Cordilleran Ice Sheet filled the SJF and processes surrounding glacial rebound formed the present coastal bluffs (Dethier et al., 1995). Eroding coastal bluffs provide sediment to the beach and to the Elwha River delta on the eastern edge of Freshwater Bay (Warrick et al., 2009). The 35m high bluffs landward, and directly south of, Freshwater Bay comprise Pleistocene glacial deposits with the face of the bluff mapped as Quaternary mass-wasting deposits (Schasse 2003; Polenz et al., 2004). The Elwha delta itself is Quaternary alluvium transported and deposited by the river (Schasse, 2003; Polenz et al., 2004).

Observatory Point is Eocene Crescent Formation marine pillow basalt with basalt breccia and volcaniclastic conglomerate and sandstone (Schasse, 2003; Polenz et al., 2004). An east-west vein of Eocene tuffaceous rock crops out at Observatory Point (Schasse, 2003; Polenz et al., 2004). This vein comprises tuffaceous sedimentary rock, water-laid tuff, and mudflow breccia (Schasse, 2003). There is an outcrop of Pliocene-Oligocene marine sedimentary rock near the mid-point of the FWB bluffs (Fig 2) (Schasse, 2003; Polenz et al., 2004).

Slope Break Formation

The rising tide tends to quickly cover the low-tide terrace because of its low gradient (Komar, 1976). When the rising water level reaches the slope break (SB) and the steeper gradient of the upper intertidal, lateral advance slows while water depth continues to increase over the low-tide terrace. Western FWB is a composite beach according to Jennings and Shulmeister's (2002) description. When water depth on composite beaches increases, the wave regime changes from spilling to plunging and from dissipative to reflective (Jennings and Shulmeister, 2002). This suggests that the SB is the most seaward point of plunging wave/sediment interaction (Wang et al., 2003; Kobayashi and Lawrence, 2004). The jet of the plunging wave suspends the sediment and then expends the rest of its kinetic energy as it rushes up the beach face (Kobayashi and Lawrence, 2004). The returning downrush, or backwash, of water from the steeper landward beach face carries the sediment seaward and deposits it on a shore-parallel bar (Kobayashi and Lawrence, 2004). The beach surface is locally depressed at this location and is not representative of the change in slope, but of the wave energy conditions of a previous flood tide.

Study Area

Jennings and Shulmeister (2002) divide coarse-grained beaches into mixed sand-and-gravel, composite, and pure gravel. Mixed sand-and-gravel beaches are less studied than sand or gravel beaches and are identified visually by the intermixing of gravel and sand in both cross-shore and vertical directions (Jennings and Shulmeister, 2002). Composite beaches tend to have coarse berms and sandy foreshores (Jennings and Shulmeister,

2002). Gravel beaches are exclusively gravel or cobble sediments (Jennings and Shulmeister, 2002). FWB has composite, mixed sand-and-gravel, and beaches that are predominantly gravel. Even though the upper beach slope fronting Coville Creek (Fig 2) and eastward past the marine sedimentary outcrop (Schasse, 2003; Polenz et al., 2004; Warrick et al., 2008) mentioned in the previous section is almost exclusively gravel and cobbles, I will not address gravel beaches for the following reason. The area around Coville Creek has the appearance of a lag apron and the sedimentary outcrop that directly underlies this apron (Warrick et al., 2008) removes it from consideration as a strictly gravel beach.

Using Jennings and Shulmeister's (2002) classifications, Miller (2011) defines the eastern portion of Freshwater Bay as a mixed sand-and-gravel (MSG) beach. MSG beaches are more likely to have a moderate-steep beachface, plunging wave regime, swash zone somewhat coarser than storm berm, wider D_{50} range (D_{50} is the 50^{th} percentile of sediment grain size on the beach), and have comparatively lower slope, though not as low as fine-grained (sand) beaches (Jennings and Shulmeister, 2002).

Western FWB is characteristic of the composite beach under Jennings and Shulmeister's (2002) system though some areas could be classified as MSG. FWB has a distinct SB, sand-dominated below the SB, gravel-dominated above the SB, dissipative low-tide terrace, and reflective high tide beach face. The dissipative low-tide terrace with its very low slope leads to spilling breakers (Komar, 1976) rather than the plunging breakers found on the MSG beach in eastern FWB.

Miller et al. (2011) tracks longshore transport by placing Radio Frequency Identification (RFID) tracers in three grain-size classes: 32-64 mm, 64-128 mm, and 128-256 mm. It is worth noting that smaller gravel and sand are not represented in these categories due to constraints imposed by mechanical insertion of the RFID tags (Miller et al., 2011). These tracers were then distributed on the Elwha delta at central, eastern, and western deployment sites (Miller et al., 2011). The western site showed movement both eastward and westward with about 60% of movement in a westward direction (Miller et al., 2011). The central and eastern sites indicate an eastward transport preference of >80% at the central site and >90% at the eastern site (Miller et al., 2011). The profile and sediment grain size of the beach surface change on annual, seasonal, and perhaps even daily scales (Miller et al., 2011).

Sediment transport on the eastern face of the Elwha delta varies between 1-173 m^3d^{-1} (Miller et al., 2011). This transport is correlated with significant wave heights of 0.3-1.2 m and disturbance depths are ~22% of the significant wave height (Miller et al., 2011). Sediment transport on the eastern face is confined to the area above the slope break (Warrick et al., 2009; Miller et al., 2012).

The seafloor in FWB is bedrock or coarse-grained, meaning sand to boulder, with shore parallel variation in boulder abundance (Warrick et al., 2008). Seaward of a chord line from the Elwha delta to Observatory Point (Fig 2), the seabed is coarse-grained with low boulder abundance (Warrick et al., 2008). Just landward of this chord line is a coarse

sediment zone of medium boulder abundance (Warrick et al., 2008). Farther shoreward of this zone is an area of high boulder abundance and coarse sediment (Warrick et al., 2008). Not mentioned in the text, but visible in Warrick et al.'s (2008) figure is a tongue of coarse sediment with medium boulder abundance that extends shoreward through the high abundance boulder zone. This tongue is roughly parallel with the incident dominant wave direction and positioned seaward of the lee zone formed by Observatory Point.

Two cuspate features in FWB's central shoreline are Coville Creek (Schasse, 2003) and a bedrock outcrop (Schasse, 2003; Warrick et al., 2008). Sand is found at both the eastern and western extremities of FWB (Warrick et al., 2008).

Previous studies indicate a dominant wave direction of 311° with standard deviation of 11° (Warrick et al., 2009; Miller et al., 2011). Peak wave period has a bi-modal distribution of 10 seconds and 4 seconds with the longer period attributed to ocean swell and the shorter period attributed to local wind-generated waves in the SJF (Warrick et al., 2009). The chord line across the embayment is approximately 5.5 km in length and trends 278° (Fig 2). The approximate depth of bathymetric contours at this chord line is 20m (Warrick et al., 2009).

Methods and assumptions

Wave Period

The period of the highest energy waves is defined as the dominant wave period (NOAA, 1996). The dominant period of waves recorded at two National Data Buoy Center (NDBC) moored buoys between 2010-2014 provides the SJF wave data. Neah Bay Buoy #46087 is located at the western end of the SJF in a water depth of 257 m (NDBC, Fig 1). New Dungeness Buoy #46088 is located near the eastern end of the SJF in a water depth of 119 m (NDBC, Fig 1).

Characteristics of waves at the dominant wave period are used to determine dominant direction. A direction histogram with 32 bins is plotted on a compass figure with length of section representing frequency of occurrence (Fig 3a). Two 20-minute sampling periods each hour lead to a possible 17520 data points per year; a frequency of 8000 indicates ~50% of the time in that year, and 4000 indicates conditions that occur during ~25% of the year.

During the four years of data for this study the Neah Bay buoy (NDBC #46087) does not have a continuous record for any single year while the New Dungeness buoy (NDBC #46088) is nearly complete. My solution was to convert 2012 and 2013 timestamps to coincide with the 2011 timestamp and plot their wave height concurrently to obtain a graphic representation of the wave regime (Fig 4). While this provides an understanding of wave regime at the buoy, it disallows the use of statistical representation since some portions of the year are represented twice, or even three times, while others are only represented once. Because of this, I can't evaluate inter-annual variation at the western end of SJF. Gaps in data could be due to frequent equipment malfunction in the high-energy western entrance to the SJF or perhaps to conditions exceeding the ability of the instrument to record data. Regardless, the New Dungeness buoy provides an almost uninterrupted four-year stretch of wave conditions that shows the seasonal wave energy pattern in the eastern Strait of Juan de Fuca (Fig 4).

An underwater (~10 m water depth) instrument tripod was placed in the eastern portion of FWB on multiple occasions by the United States Geological Survey (USGS) to record data before, and during, the removal of the Elwha and Glines Canyon Dams. I used the wave height, average wave period, and the approach direction of the waves associated with the average wave period recorded from Dec. 2010 through Sept. 2011 for this paper. The USGS data only covered two ~4-month deployments instead of an entire year. I joined these into one set and compared it with the same 9-month window for the Neah Bay and New Dungeness buoys, though the Neah Bay buoy only had 5 months of data in this window (Fig 5).

Wave Height

Significant wave height is the average of the highest one-third of waves recorded at an instrument location and is used to calculate wave energy (NOAA, 1996). To derive wave energy density and wavelength, I used small amplitude wave theory. Use of this theory assumes small wave amplitude compared to wavelength and water depth (Sorensen, 1993). Approximating waves in shallow water or large waves at sea are outside the

bounds of this theory (Sorensen, 1993). At Neah Bay and New Dungeness buoys this approximation is valid, and, though it holds less validity at the USGS tripod, it is accurate enough for my purpose (Sorensen, 1993).

Plotting wave energy density (Equation 1) over time reveals that two apparent wave regimes exist. I used 4 kJm^{-2} as a threshold value between summer and winter conditions at the New Dungeness buoy. This value was frequently exceeded during the winter and rarely approached during summer (Fig. 4). I did not attempt to determine a threshold level for activation and transport of a specific grain size. Rather, I chose an arbitrary value from the four years of data at the New Dungeness buoy that separated the higher energy values of the winter and spring from the lower values of the summer and early fall. The data from the Neah Bay buoy neatly resolves into two regimes with the same time bounds. The higher wave energy at Neah Bay increases the threshold level to 15 kJm^{-2}, however.

I color coded the profile graphs so that winter profiles are easily distinguished from summer profiles and looked for correlation between wave energy density regimes and profile elevation.

Calculations

The only wave parameters used are the dominant period, direction of the dominant period wave, and the significant wave height. Wave energy scales with the square of height (Sorensen, 1993), so all heights are converted to wave energy density using:

$$E = \frac{\rho g H^2}{8}, \qquad (1)$$

Where E = wave energy in kJm^{-2}, ρ is water density (1032 kgm^{-3}), g = 9.81 ms^{-2}, and H = significant wave height. Water density in the SJF varies with depth, east-west location, and also from center-channel to the shoreline (Masson and Cummings, 2004). The density given here is a general value based on Masson and Cummings (2004) representation of the western Strait of Juan de Fuca. This generalization is acceptable since variations in salinity, which is the largest driver in density, in SJF represent <1% of the density value used.

I calculated wavelength for both "deep" and "shallow" conditions. Under "deep water" wave conditions, meaning

$$d > \frac{\lambda}{2}, \qquad (2)$$

where d = water depth and λ = wave length, wavelength is defined as

$$\lambda = \frac{gT^2}{2\pi}, \qquad (3)$$

where g = 9.81 ms^{-2}, π = 3.1416, and T = wave period. To determine wavelength under "shallow water" conditions, meaning

$$d < \frac{\lambda}{20}, \qquad (4)$$

wavelength is

$$\lambda = T\sqrt{gd}, \qquad (5)$$

where the variables are consistent with previous use.

Assumptions

Assuming the depth of SJF west of the Elwha delta is 175-200 m (Davenne and Masson, 2001), and assuming deep water conditions (Equations 2 and 3), any wave period less than 15 seconds will act as a deep water wave until it begins to shoal against the edges of the Strait. Given the mean values in Table 1, mean wavelength at Neah Bay will begin to shoal in 83 m water depth and mean wavelength at New Dungeness will shoal at 18 m water depth (Equation 2 and 3).

A different situation exists for the Elwha delta tripod. A deep water wavelength of 49 m (Equations 2 and 3) and a shallow water wavelength of 54.6 m (Equations 4 and 5) are given in Table 1. A calculation for intermediate water depth is the range between these two, so these give the bounds for wavelength calculated from mean period (Table 1) at the tripod location. Since both of the given wavelengths will begin to shoal at ~25 m water depth (equation 2), and the tripod is located at 9.78 m depth, the mean wavelength will always be shoaling when it reaches this depth (Equations 2 and 4). In fact, for a wave to just begin shoaling at the tripod's depth it would need to have a wave period less than 2.02 seconds (Equations 2 and 3). The minimum wave period recorded at the tripod (Table 1) is 2.2 seconds, so presumably the mean wave at the tripod is always shoaling.

Since the nearshore tripod covers a much shorter time span, I used it to establish a data window for comparison (Fig 5). Also, I converted the USGS data to the same time base as the NOAA buoys. Even so, Buoy #46087 only has viable data for the latter five months of this window.

Beach Profile

Dave Parks, with Washington State Department of Natural Resources (DNR), used a Real Time Kinematic Global Positioning System (RTK-GPS) to characterize the profile of four cross-shore transects in FWB. Parks recorded this data 3-7 times per year between 2010-2014, excluding two instances when two profiles were collected, three instances when one profile was collected, and one instance when no profiles were collected.

Foreshores like FWB have low-tide terraces with a low slope and an upper intertidal with a greater slope. The low-tide terrace tends to dissipate wave energy and the upper intertidal reflects some of the wave energy (Komar, 1976). The SB is the point where these two planes meet. Slope Break (SB) does not have a uniform position vertically or horizontally. I visually determined the SB on the profile as the point with the greatest change in slope.

On some profiles a trough and seaward ridge feature was apparent at the SB profile. Under these circumstances, I defined the point at the landward edge of the trough as the SB. The trough is formed under a plunging wave regime (Wang et al., 2003; Kobayashi and Lawrence, 2004).

Surface Sediment Expression

Concurrently with the elevation data, Parks collected digital images of the bed sediment at various points along the profile transect. Images are more closely spaced in the upper intertidal and farther apart in the lower intertidal. Transect endpoints were located and then data was collected at meter intervals along a tapeline. In some instances a U.S Customary tape was used with units of feet, but all were converted to meters (1 meter = 3.28 feet) for profile display. As a result, some increments are decimal meters instead of whole meters.

Three positions along each profile were compared through time for changes in cross-shore location and grain size. Mean High Water (MHW), Mean Sea Level (MSL), and Mean Low Water (MLW) are elevation datums relative to the North American Vertical Datum of 1988 (NAVD 88). Given the necessity of completing two profiles within one low tide cycle, it was not possible to locate these points exactly during sampling. After each profile was graphed, the image closest to each reference location was chosen as representative of that datum.

Images were then processed using a statistical auto-correlation program written for Matlab (Buscombe et al., 2010). The autocorrelation yields a mean grain size for a 10 cm square crop of the image but not a grain size distribution for either the crop or the whole image.

The auto-correlation program requires that a series of three steps be performed on each image (Buscombe et al., 2010). The first step is to establish a correlation coefficient between pixels and millimeters. Following prompts by the program, I marked 100 mm on the scale included in each photo; in instances where the scale was unclear, 10 cm was marked on the transect tape. The second step is an image crop of an approximately 10 cm square area for processing. From this cropped image the software determines a mean grain-size based on pixel intensity. The final procedure is to multiply the correlation coefficient by the pixel-based grain size to attain a calculated grain size in millimeters.

Problems with this method include: the small crop size, differences in reflectivity due to moisture, direct light sources in the field that introduce a large degree of shadowing, difficulty representing images with a bi-modal distribution, and the difficulty of picking a cropped region that is representative of the image. As mentioned previously, the crop size for this program is 10 cm square and, since many of the images were strongly bi-modal in nature, the results of the autocorrelation analysis were not representative of the observed grain size. Some of the images were obtained during nighttime fieldwork and these images often have highly reflective regions and have shadows that are larger than anticipated by the developers of the program (Buscombe et al., 2010). An image that is

exclusively gravel could have the same mean grain size as an image with a bi-modal distribution of sand and cobbles. The minimal crop size raises difficulties when cobbles are part of the image, since the cropped image can be smaller than the dominant sediment grains.

Comparing the dominant grain size with the scale or the transect tape in each image I categorized sediment as: cobble, gravel, sand, and sand-with-fines. I used standard boundaries at 64 mm, 4 mm, and the presence of ripples to separate sand and sand-with-fines (defined below). Small differences in grain size like medium sand to coarse sand, or pea gravel to gravel, are not differentiated with this process. For images with a bi-modal distribution I made an estimation of coverage by grain size.

Sand-with-fines (combined silt and clay <0.063 mm) may not be factually correct, since Warrick et al. (2008) find no areas in FWB with low sonar backscatter as would be expected with mud. Sand on the higher slope above the SB appears coarser in the images, appears to have more pore space, and doesn't form ripples. Sand on the lower slope below the SB appears finer, retains water in low spots, and forms ripples. I used sand-with-fines to distinguish between the two facies realizing that there may not actually be fines in the sand; it may instead be sand with a sizable fraction of finer sand.

To introduce a method of uniformity and to remove bias, I compared grain size at four readily identifiable positions, MHW, MSL, MLW, and SB (Tables 2 and 3). For MHW, MSL, and MLW, I used fixed vertical values of 2.0 m, 1.3 m, and 0.6 m, respectively. These values are referenced to Mean Lower Low Water (MLLW) at NDBC Station #9444090 in Port Angeles, Washington. The characteristics I use to define the SB have been described in the middle section in the background portion of this paper.

Results

Waves—Buoy #46087, Neah Bay

The highest frequency of dominant wave period at Neah Bay (Buoy #46087) is due West through West North West (Fig 3). From early May until mid-Sept., Buoy #46087 peak wave energy density is consistently below 5 kJm^{-2} with occasional forays to 15 kJm^{-2} (Fig 4). From mid-Sept. through April peak wave energy density is frequently above 10 kJm^{-2} and regularly exceeds 40 kJm^{-2} (Fig 4). Due to gaps in the data, any compilation over-represents Oct. through Dec. and underrepresents mid-March through June. Because of this, I didn't attempt a statistical analysis—results are qualitative rather than quantitative—but imply a summer low-energy period and a winter high-energy period. This idea is corroborated by data from Buoy #46088.

Waves—Buoy #46088, New Dungeness

At New Dungeness (Buoy #46088) the direction of dominant wave period varies between due West and West South West, with a secondary peak East South East (Fig 3). The New Dungeness buoy has a nearly complete data record for the four years that this study covers (Fig 4). New Dungeness has a decrease in peak wave energy density from mid-May through Sept. In the four-year span of this dataset 4 kJm^{-2} is approached nine times and exceeded on only four occasions during the low-energy regime. Generally, the peak wave energy density during the low energy regime is less than 2 kJm^{-2}. By Nov., 4 kJm^{-2} is exceeded many times each month, with values regularly above 8 kJm^{-2} and one instance in 2010 that approached 14 kJm^{-2}.

Waves—USGS tripod, Elwha Delta

The USGS instrument tripod shows a reduction in wave energy density akin to the decrease at New Dungeness (Fig 5). Generally, the energy is less than 2 kJm^{-2} with occasional spikes to 4 kJm^{-2}. This dataset only extends from mid-Dec. 2010 through the middle of Sept. 2011. As such, only 50% of the high-energy period from Oct. through April is represented (Fig 4).

Waves—Mean Wave Period

Mean wave period is 10.3 seconds (Table 1) with a normal distribution at Buoy #46087 (Fig 6). The mean wave period at buoy #46087 has a wavelength of 165.6 m (Equation 2 and 3) and a wave height of 1.7 m (Table 1). Both Buoy #46088 and the USGS tripod have a right-tailed distribution (Fig 6). The mean wave period for Buoy #46088 and the instrument tripod is 4.8 seconds and 5.6 seconds, respectively (Table 1). The mean wave period at Buoy #46088 has a mean wavelength of 36 m (Equation 2 and 3) and a mean wave height of 0.4 m. The USGS tripod has a mean wavelength between 49-55 m (deep- and shallow-water derivations, respectively, Equations 2, 3, 4, and 5) and a mean wave height of 0.48 m.

Waves—Derived Values

Wave energy scales with the square of wave height (Komar, 1976; Sorensen, 1993). The Neah Bay dataset does not include the high-energy period from Jan. through mid-April, so it is likely that wave energy density in Table 1 is low for the Neah Bay buoy. Comparing the energy of the mean wave height (Table 1) shows the USGS instrument

tripod location receiving 80%, and New Dungeness receiving 55%, of the mean wave energy recorded at Neah Bay. With a wave regime near the mean period, the Elwha delta tripod receives 45% more wave energy than the New Dungeness buoy. In contrast, for maximum wave energy conditions, New Dungeness receives 14.8%, and the tripod receives 8.3%, of wave energy at Neah Bay. For maximum conditions, then New Dungeness receives 80% more wave energy than the USGS tripod in eastern FWB.

Wave length scales directly with wave period for shallow water waves (Equation 5) but with the square of wave period for deep-water waves (Equation 3) (Komar, 1976). The deep-water relationship is shown by Buoy #46087 having slightly more than twice the mean wave period of Buoy #46088 but more than four times the calculated mean wavelength (Table 1).

Beach Profile

Profiles of four transects in Freshwater Bay were recorded 2010-2014 (Figs 7-10). The frequency varies from year-to-year and from transect-to-transect, with a maximum of seven profiles for T1 in 2011 (Fig 7) and the minimum in 2014 for T2 (Fig 10) when no profiles were recorded. Profile elevations have their origin at Mean Lower Low Water (MLLW) as defined for the NDBC Station #9444090 (PTAW1) at Port Angeles, Washington.

All bar and trough features will be referred to as ridge-and-runnel; the sandbar is the ridge and the trough is the runnel. Following Komar's (1976) definitions, longshore bars occur seaward of the breaker zone, while ridge-and-runnels form on a low-tide terrace. T1 and T2 have a low-tide terrace, T3 appears to have a low-tide terrace, but is possibly a planar bedrock outcrop covered in cobbles and gravel (Warrick et al., 2008). T4 could have longshore bars but the SB and potential terrace were rarely reached during surveys (Fig 10).

Eastern FWB is orthogonal to the dominant wave regime and prominent examples of cusps form there (Wash. Coastal Atlas, 2002, 2006). The two most recent series of aerial images show recognizable cusps, indicating that their formation must be relatively frequent (Wash. Coastal Atlas, 2002, 2006). This view was reinforced by a field visit I made to FWB on January 28, 2015. Cusp development was noticeable along the entire eastern curve of FWB, westward through the small embayment before Coville Creek, and some way westward of Coville Creek. These cusps were primarily gravel around Coville Creek, but nearer to the Elwha delta the cusps were coarse sand and gravel. In the eastern portion of FWB, cusps were formed at different elevations. On both sides of Coville Creek, cusps and embayments were only visible near MHW.

Transect 1 (T1) shows summer profiles regressed landward when compared to winter profiles in 2010 (Fig 7a). The profiles on July 11, 2011 and July 28, 2011 show deposits of ~0.5 m of sediment below the SB and substantial increase in elevation above the SB (Fig 7b). The surface sediment after the aggradation is primarily sand-with-fines, but some gravel and cobble are present (Fig 12). A large deposit in Dec. 2011, not visible in the July 2011 profile, is evidence of a bluff failure (Fig 7b). March and June profiles in

2012 show the remains of the deposit working their way down the beach face (Fig 7c). There is no obvious evidence of the deposit by Dec. 2012 save for a convex appearance to the beach above MHW (Fig 7c). The convexity is removed by May 2013, but a convex appearance returns by Aug. and Dec. 2013 (Fig 7d). Plunge points with seaward build-up of displaced sediment are only visible for the Aug. 6, 2010 and the Dec. 26, 2013 profiles (Fig 7a and 7d). In addition, the SB during 2013 experiences elevation loss of 0.64 m between Aug. 18, and Dec. 26. Figure (11) shows that cobble is the dominant size fraction in both images.

All four profiles for Transect 2 (T2) in 2010 show plunge points and seaward-displaced sediment (Fig 8a). In 2011, only April 18 shows a plunge point and displaced sediment, though Feb., April, May, and July all show shore parallel ridges between 40-60 m cross-shore distance (Fig 8b). Three profiles in 2012 show neither plunge points nor shore parallel bars (Fig 8c). All three profiles in 2013 show a ridge at 55 m indicating persistence for seven months or the ability to re-form in the same place consistently (Fig 8d). All three 2013 profiles also show at least one additional ridge-and-runnel feature shoreward of the prominent one previously mentioned (Fig 8d). In addition, the May profile shows a ridge-and-runnel located 80 m cross-shore (Fig 8d).

Transect 3 (T3) shows a marked increase in the slope of the low-tide terrace below the SB (Fig 9a-9e). There is regression in 2010 from the July profile to the August profile in the upper intertidal (Fig 9a). The upper intertidal progrades through Oct. and has a Dec. profile that is essentially identical (Fig 9a). Ridges are evident at 30 m in Oct. and Dec. and at 53 m in Aug (Fig 9a). The shore face is slightly prograded in Feb. 2011 and this remains stable through July (Fig 9b). A ridge-and-runnel is visible at 45 m in May and has moved shoreward to 38 m in July (Fig 9b). A ridge-and-runnel is visible at 65 m cross-shore in 2012 (Fig 9c). Also, a pronounced berm at 3 m elevation is visible in 2012 and is consistent with sediment deposited in the upper intertidal (Fig 9c). In addition, below the SB an increase in elevation out to 50 m cross-shore shows substantial deposition (Fig 9c). This increased elevation is maintained through 2014 (Figs 9c-9e). Profiles in 2013 show the first evidence of plunge points and shore-parallel bars at the SB (Fig 9d). This is obvious in Jan., not visible in May, and makes a return in July (Fig 9d). Ridge-and-runnels are visible seaward of 50 m in both May and July (Fig 9d). By 2014, June shows an elevated shore face above MHW while Sept. shows a plunge point at the SB and a ridge-and-runnel at 60 m (Fig 9e).

Transect 4 (T4) rarely extends seaward far enough to identify the slope break. The July 2010 to Dec. 2010 profiles show uniformity below MHW with slight aggradation through the profile sequence (Fig 10a). There is much more variation above MHW in 2010 (Fig 10a). There are four 2011 profiles from March through July 2010 (Fig 10b). This set of profiles exhibits noticeable conformity and shows a large persistent convex feature above MHW (Fig 10b). The single profile for 2012 was recorded in June and shows aggradation along the entire profile and a pronounced berm at 4 m cross-shore (Fig 10c). This increased elevation is continued in the profiles that range from Jan. 2013 through the end of Nov. 2013 (Fig 10d). A loss of sediment is visible below MHW and a mobile convex feature at 3 m elevation moves landward over the course of the year (Fig 10d). The

following year, 2014, there is high uniformity through most of the profile length with ~0.5 m elevation increase at 5 m cross-shore (Fig 10e). A ridge is evident at 48 m cross-shore in June and possibly at 46 m in September (Fig 10e).

Inter-Transect Trends (Figs 7-10)
These four transects originate at either the base of the bluff that backs the beach or at the seaward edge of the berm crest. In both cases, this is the highest elevation that up-rushing waves reach. The elevation of the transect origins increases in the eastward direction from 3.25 m at Transect 1 to 4.25 m at Transect 4. Transects 1 and 2 have lower gradient shore faces below the SB and extend much farther seaward than Transects 3 and 4.

Intra-Transect Change in MHW, MSL, MLW, and SB (Q1-10 = 1st quarter 2010)
T1 MHW and MSL aggrade Q3-10 through Q4-10, with a quick regression and recovery at Q2-11. MLW is noticeably seaward through this time (Fig 13). Some variation is exhibited through the beginning of Q3-11 and then some stability through Q2-13. The end of Q3-13 shows a 20m seaward extension of MLW. By Q1-14, MHW, MSL, and SB have withdrawn and MLW has returned 15m. After this, MHW, MSL, and SB return to the same location as Q3-11 through Q2-13, but MLW is seaward of the trend.

T2 has seaward extension of MLW from Q3-10 through Q4-10, mid-Q2-11 through Q2-12, end of Q4-12, and end of Q3-13 through Q1-14 (Fig 14). The landward movement of MLW each spring (Q2-11, Q2-12, and Q2-13) accompanies the seaward movement of SB. An event from the end of Q1-11 through the beginning of Q2-11 indicates substantial regression (~5 m cross-shore) of MHW, MSL, and MLW and seaward extension of SB.

T3 shows MHW, MSL, MLW, and SB stable through Q2-11 (Fig 15). At this point MLW progresses seaward by ~10m and maintains that position. MHW and MSL remain roughly parallel through the rest of the recorded time period, showing a general increase through Q2-13, with a parallel regression in Q3-13. SB is consistently seaward of MHW and MSL until Q3-11. No data are recorded until Q2-12 when SB migrated shoreward of MSL, where it remains until late in Q1-13. SB parallels the progression of MSL and MHW in Q2-13 and then resumes its place seaward of MSL.

T4 has almost no SB data points so this just concerns the movement of MHW, MSL, and MLW (Fig 16). MHW shows a substantial regression at the end of Q4-10. A paucity of data points for MSL and MLW at that time makes comparison impossible. MHW, MSL, and MLW all prograde through Q2-12 and maintain that position through Q3-13. All three show slight regression at Q3-13, with an equilibrium pattern through Q3-14.

Discussion

All four transects show evidence of sediment deposition and removal through time. The eastern transects show deposition that could be attributed to an increase in sediment delivery to the shoreline after the removal of two dams on the Elwha River. This is in agreement with the findings of Gelfenbaum et al. (2015) who find increased sediment deposition in eastern FWB post-2011 dam removal. The two western transects show transient episodes rather than long-term trends in deposition. Also, the western transects show high variation prior to, and the eastern transects are more stable prior to, the 2011 dam removal.

Eastern Freshwater Bay

Both transects in eastern FWB exhibit sediment accretion after 2011. Transect 3 shows a persistent seaward extension of MLW by nearly 10 m between July 2011 (Q3-11 in Figure 15) and Jan. 2013 (Q1-13 in Figure 15). The beach face above the SB also aggrades seaward during this period indicating that sediment is being deposited across the entire intertidal after the removal of the Elwha River dams began in 2011. Transect 4 shows accretion in the upper intertidal over the same period with a slight regression in June 2013, (Q2-13 in Figure 16). There is no record of an equivalent increase in the low-tide terrace since profiles at this transect rarely extend that far.

Since cusps are common along the section of shoreline where T3 and T4 are located, it is possible that some of the profile changes here are lateral migrations of cusps and embayments through the transect line and do not represent overall transect progradation or regression. A likely cusp feature is persistent at 3-18 m cross-shore from March 21, through July 11, 2011 (Fig 10b). Komar (1976) relates that the best conditions for cusp formation are regular wave crests (not confused seas) parallel to the beach. It is believed that cusp formation is co-incident with cross-shore transport rather than longshore transport (Komar, 1976), though one is not exclusive of the other. This idea is reinforced by the findings of Miller et al. (2011) that showed minimal net longshore transport on this shoreface. Since incident dominant wave rays are orthogonal to this shoreline (Figs 1 and 3a), cross-shore transport is the presumed driver of the observed cusp formation.

Western Freshwater Bay

There is not an equivalent trend of sediment accretion in western FWB. The low-tide terrace in both T1 and T2 experiences transient sediment deposition or erosion throughout the period of this study. They differ in that T1 appears to have sediment periodically deposited and then quickly carried away, as evidenced by the seaward extension of MLW from 20 m cross-shore to 40 m cross-shore and subsequent immediate return to near the SB at 20 m (Fig 13). In contrast, T2 has a MLW position that hovers near 40 m cross-shore and occasionally regresses to near the SB at 20 m cross-shore (Fig 14). This is also transient, but in an opposite sense from T1, in that MLW quickly returns to near 40 m cross-shore.

This leads to the assumption of T1 as an area with relatively stable topography that undergoes periodic deposition, either from infrequent bluff failure above the SB or from oceanographic processes below the SB. The sediments below the SB appear to pass

through quickly and be replenished slowly. Where this sediment comes from is not known, but could conceivably be sediment carried west by the less frequent NE wind-generated waves that can be seen in the data from the USGS tripod (Fig 3b). If this were the case, then this sediment is probably sourced from the Elwha delta.

Taken together these transects are suggestive of possible eastward-moving sediment moving quickly across the far western portion of FWB (T1) and then moving more slowly across the still western, but more central portion (T2).

Slope Break

Frequently, the features referred to as ridge-and-runnel occur at the Slope Break which, strictly speaking, is not the low-tide terrace, but rather the transition point to the upper inter-tidal. This feature is formed when the advancing tide is slowed by the increase in beach gradient, the wave form changes from spilling to plunging due to increased water depth as the tide continues to rise, the plunging breakers disturb sediment, and gravity flow from the uprush of the previous wave carries this sediment seaward (Wang et al., 2003; Kobayashi and Lawrence, 2004). Since the energy of plunging waves is concentrated here, it follows that this is the location most likely to experience significant changes in either elevation or grain size composition.

The 0.64 m decrease in elevation at Transect 1 during the final five months of 2013 shows that cobble-size sediment is being removed at the SB or that the winnowing of finer grains results in undermining and decreased elevation for resident cobbles (Figs 7d, 11A, and 11B).

An event in July 2011 shows 0.5 m of sediment deposited along the entire profile face over a 17-day period. The exposed surface sediment after this event includes gravel and small cobble (Fig 12). It is unknown if this event occurred in one tidal cycle or is cumulative over the 17-day interval.

Since the July 2011 event occurred during the low-energy wave regime, it is reasonable to assume that substantial volumes of sediment move throughout the year. Since cobbles and gravel were part of both the 2011 and the 2013 events, it is reasonable to assume that all of the sediment up to, and including, cobble is mobile in the intertidal of FWB throughout the year. Figure 4 shows wave energy density data for the years 2010-2013 and careful inspection reveals a spike in mid-July 2011 of slightly more than 4 kJm^{-2}. If this event caused the increase in elevation, it would imply that the threshold level of 4 kJm^{-2} that I arbitrarily chose to differentiate winter and summer conditions is still energetic enough to move large volumes of sediment.

Changes in elevation at all four transects throughout the year indicate that sediment is transient both above and below the slope break. The direction of movement is not known, but all long-term indicators above MHW suggest an eastward direction of transport. Even the boat ramp near the far western end of FWB shows a tongue of sand and smaller gravel pointing eastward. Shoreline features in the upper inter-tidal of western FWB (T1 and T2) indicate that littoral transport is toward the east. An easily visible indicator is the

small sandspit extending eastward and offsetting the mouth of Coville Creek (Wash. Coastal Atlas, 2002, 2006). In addition, landslide-deposited tree trunks with attached root masses pivot their tips towards the east (Wash. Coastal Atlas, 2002, 2006). This is an indicator of predominant wave direction rather than longshore transport, but, since the predominant waves carry sediment, it supports the idea of eastward transport in western FWB.

Ridge-and-runnel features are visible in all four transects and during both low-energy and high-energy wave conditions. Transect 4 only has evidence of this in 2014 (Fig 10e). Transect 2 is the only one that shows the apparent persistence of a ridge feature throughout the year, or at least from May through Dec. of 2013 (Fig 8d). The impermanence of shore parallel ridge-and-runnels also suggests a highly mobile topography in FWB.

Only one presumed bluff failure was recorded in these profiles—the Dec. 20, 2011 large deposit above MHW (Fig 7b). It seems improbable to have a bluff failure occur at a transect location. Because of the infrequency of surveys, both temporally and spatially, no estimation of coastal bluff contribution to the sediment budget of FWB is possible.

Freshwater Bay Wave Energy

The proportion of wave energy measured at the Neah Bay buoy that reaches the Elwha River delta and the New Dungeness buoy is dependent on the wave parameters. It is apparent that during mean wave conditions only 69% of the wave energy that reaches the USGS tripod is evident at the New Dungeness buoy. In contrast, during maximum wave conditions, 78% more wave energy is measured at the New Dungeness buoy than at the tripod. This is due to differences in water depth at each location. The greater water depth at the New Dungeness buoy allows longer period waves to propagate farther eastward, in contrast to the USGS tripod's shallower depths that cause larger waves to steepen and break seaward of the tripod location (Komar, 1976; Sorensen, 1993). In addition, the tripod has 40% more wave energy density at minimum conditions. This can be attributed to shorter period waves increasing in height as they shoal in the shallower water (Komar, 1976; Sorensen, 1993), while those same waves maintain a lower height at New Dungeness in the absence of shoaling.

This implies that the instances of greatest sediment movement in FWB may not occur during the periods of highest wave energy density measured at either New Dungeness or Neah Bay. The offshore bathymetry may serve to attenuate the highest wave energy densities before they impact the shoreline.

Conclusion

Even though there is a noticeable decrease in wave energy density from May through Sept., there is still enough energy to effect significant changes in the intertidal elevation profile of Freshwater Bay.

In addition to changes in the profile, grain sizes from sand through cobble are mobile in FWB, or at least are mobile at the slope break in FWB. Sand through cobble can be deposited or removed in a matter of weeks, and can happen at all times of the year.

The beach face of Freshwater Bay is highly mobile above and below the slope break. The most western portion of Freshwater Bay has periodic depositional events that are quickly transported elsewhere. Just west of Coville Creek in central Freshwater Bay, T2 appears to be a short-term reservoir for sediment. In this section of FWB, sediment is persistent, perhaps on annual scales, is transported elsewhere in short-term events, and then rebuilds quickly. Eastern Freshwater Bay is an accreting beachface, possibly due to increased Elwha river sediments.

Limitations

Buoy Data

At the time I collected data for this paper, historical data for both NDBC buoys was only compiled through 2013. Since I had relatively few profiles in 2014 (one transect had a single profile in 2014), the omission of 2014 data seemed insignificant.

Buoy #46088 is only missing short periods of data from Jan. 1, 2010 through Dec. 31, 2013. The largest omission was April 13, 2013 through April 30, 2013.

Buoy #46087 has no data for 2010, Jan. 1 through mid-April 2011, mid-March through June 2012, and May through Oct. 2013. Characterization of the wave regime at this buoy thus includes Oct. through Dec. three times, Jan. through mid-March twice, but May through June only once. Therefore, any statistics will be weighted toward the higher-energy regime that persists from Oct. through April, with a corresponding under-representation of the lower-energy regime of May through Sept. In effect, I am using one dataset to characterize the low-energy regime. There is a possibility that this dataset was unseasonably low.

I can justify the high-energy/low-energy assumption of the Buoy #46087 dataset since the complete record of Buoy #46088 also supports a division into high and low-energy regimes. The low energy regime runs from Mid-May through Sept.

Transect Profiles

Cross-shore and longshore transport are proposed in this dataset, but no transport event is attributed to a specific wave energy event. This is due to the low temporal resolution of the data.

Tides do not recede to the same level throughout the year. Very low tides occur near the winter and summer solstices. This variation in sub-aerial exposure of the low-tide terrace leads to differential length of profiles in different seasons. Therefore, some low-tide areas are only captured once per year, which makes discussion of the profile behavior impossible.

In addition, low tides during the winter solstice happen at night, making data collection difficult and leading to later processing issues when reading the transect tape measure and scale bars. Nighttime images often have more surface moisture and higher image reflectivity. One of the requirements for the Buscombe et al. (2010) image processing software is an indirect light source that limits reflectivity; this requirement is not met with nighttime images and a camera flash.

References Cited

Buscombe, D.D., Rubin, D.M., Warrick, J.A., 2010. A universal approximation of grain size from images of noncohesive sediment, J Geophys. Res. 115, FO2015, doi:10.1029/2009JF001477.

Davenne, E. and Masson, D., 2001. Water properties in the Straits of Georgia and Juan de Fuca. Fisheries and Oceans Canada, Institute of Ocean Sciences.

Dethier, D.P., Pessl, F., Keuler, R.F., Balzarini, M.A., Pevear, D.R., 1995. Late Wisconsonian glaciomarine deposition and isostatic rebound, northern Puget Lowland, Washington. Geological Society of America Bulletin 107:1288-1303.

Duda, J.J., Warrick, J.A., Magirl, C.S., 2011. Coastal and lower Elwha River, Washington, prior to dam removal—history, status, and defining characteristics, chap. 1 *of* Duda, J.J., Warrick, J.A., and Magirl, C.S., eds., Coastal habitats of the Elwha River, Washington—Biological and physical patterns and processes prior to dam removal: U.S. Geological Survey Scientific Investigations Report 2011-5120, 1-25.

Gelfenbaum, G., Stevens, A.W., Elias, E., Warrick, J., 2009. Modeling sediment transport and delta morphology on the dammed Elwha River, Washington State, USA. In: Mizuguchi, M., Sato, S. (Eds.), Proceedings of Coastal Dynamics 2009: Impacts if Human Activities on Dynamic Coastal Processes. World Scientific, Tokyo Japan.

Gelfenbaum, G., Stevens, A.W., Miller, I., Warrick, J.A., Ogston, A.S., Eidam, E., 2015. Large-scale dam removal on the Elwha River, Washington, USA: Coastal geomorphic change. Geomorphology (in press). http://dx.doi.org/10.1016/j.geomorph.2015.01.002

Jennings, R., Shulmeister, J., 2002. A field based classification scheme for gravel beaches. Marine Geology 186, 211-228.

Kobayashi, N. and Lawrence, A.R., 2004. Cross-shore sediment transport under breaking solitary waves. Journal of Geophysical Research, 109, C03047, doi:1029/2003JC002084.

Komar, P.D., 1976. Beach processes and sedimentation. Prentice-Hall, Inc., Englewood Cliffs, NJ. 429 pp.

Masson, D. and Cummins, P.F., 2004. Observations and modeling of seasonal variability in the Straits of Georgia and Juan de Fuca. Journal of Marine Research, 62, 491-516.

Miller, I.M., Warrick, J.A., Morgan, C., 2011. Observations of coarse sediment movements on the mixed beach of the Elwha Delta, Washington. Marine Geology 282, 201-214.

Miller, I.M., 2014. Four summer observations from the Elwha River Delta. The Coast Nerd Gazette, September 3, 2014. http://coastnerd.blogspot.com/2014/09/four-summer-observations-from-elwha.html

National Data Buoy Center (NDBC), www.ndbc.noaa.gov/

National Oceanic and Atmospheric Administration (NOAA), 1996. Nondirectional and directional wave data analysis procedures. NDBC Technical Document 96-01. Earle, E.D., Neptune Sciences, Inc. Slidell, Louisiana.

Parks, D., Shaffer, A., and Barry, D., 2013. Nearshore drift-cell sediment processes and ecological function for forage fish: implications for ecological restoration of impaired Pacific Northwest marine ecosystems. Journal of Coastal Research, 29(4), 984–997.

Polenz, M.P., Wegmann, K.W., Schasse, H.W., 2004. Geologic map of the Elwha and Angeles Point 7.5-minute quadrangles, Clallam County, Washington. Olympia, Washington: Open File Report 2004-14, Division of Geology and Earth Resources, Washington Department of Natural Resources, 1 sheet.

Puget Sound LiDAR Consortium, files: q48123b44, q48123b53
http://pugetsoundlidar.ess.washington.edu/lidardata/restricted/index

Schasse, H.W., 2003. Geologic Map of the Washington Portion of the Port Angeles 1:100,000 Quadrangle, Clallam County, Washington. Olympia, Washington: Open File Report 2003-6, Division of Geology and Earth Resources, Washington Department of Natural Resources, 1 sheet.

Shipman, H., 2010. The geomorphic setting of Puget Sound: implications for shoreline erosion and the impacts of erosion control structures, *in* Shipman, H., Dethier, M.N., Gelfenbaum, G., Fresh, K.L., and Dinicola, R.S., eds., 2010, Puget Sound Shorelines and the Impacts of Armoring— Proceedings of a State of the Science Workshop, May 2009: U.S. Geological Survey Scientific Investigations Report 2010-5254, 19-34.

Sorensen, R.M., 1993. Basic wave mechanics: for coastal and ocean engineers. John Wiley & Sons, Inc., New York.

Wang, P., Ebersole, B.A., Smith, E.R., 2003. Beach-profile evolution under spilling and plunging breakers. J. Waterway, Port, Coastal, Ocean Eng. 129, 41-46.

Warrick, J.A., Cochrane, G.R., Sagy, Y., Gelfenbaum, G., 2008. Nearshore substrate and morphology offshore of the Elwha River, Washington. Northwest Science, 82(sp1): 153-163.

Warrick, J.A., George, D.A., Gelfenbaum, G., Ruggiero, P., Kaminsky, G.M., Beirne, M., 2009. Beach morphology and change along the mixed grain-size delta of the dammed Elwha River, Washington. Geomorphology 111 (3–4), 136–148.

Warrick, J.A., Draut, A.E., McHenry, M.L., Miller, I.M., Magirl, C.S., Beirne, M.M., Stevens, A.W., and Logan, J.B., 2011. Geomorphology of the Elwha River and its delta, chap. 3 *of* Duda, J.J., Warrick, J.A., and Magirl, C.S., eds., Coastal habitats of the Elwha River, Washington—Biological and physical patterns and processes prior to dam removal: U.S. Geological Survey Scientific Investigations Report 2011-5120, 47-74.

Washington Coastal Atlas, Series: June 26, 2006; May 31, 2002; Elwha delta and Freshwater Bay Clallam County. https://fortress.wa.gov/ecy/coastalatlas/tools/ShorePhotos.aspx

Figures

Figure 1

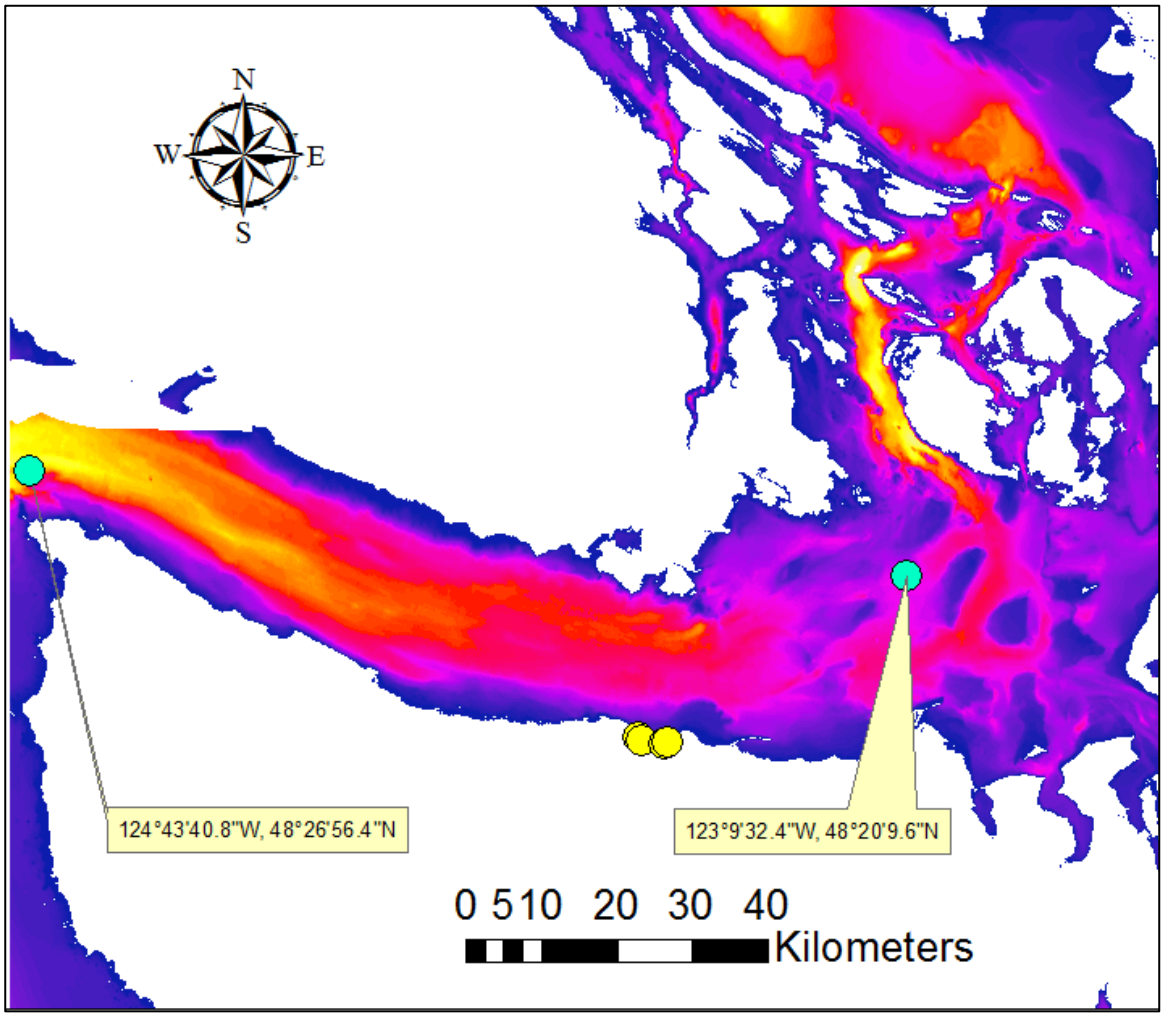

Figure 1. Strait of Juan de Fuca with bathymetric contours. Blue bathymetry is shallower and yellow is deeper. Yellow circles are location of transects in Freshwater Bay. Turquoise circles mark NDBC Buoy #46087 (124°43'40.8"W, 48°26'56.4"N) and #46088 (123°9'32.4"W,48°20'9"N).

Figure 2

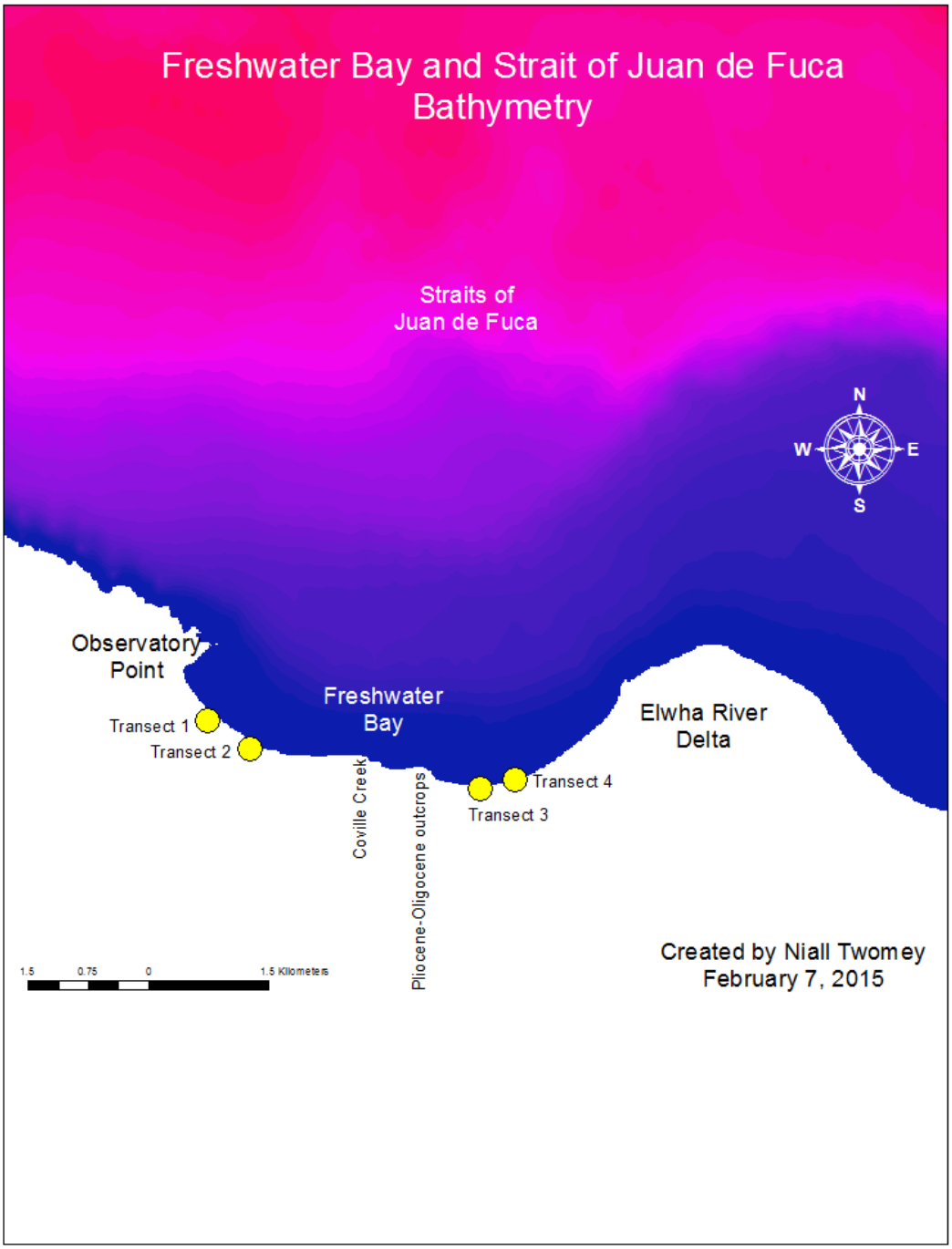

Figure 2. Freshwater Bay and Transects 1-4 with Observatory Point to the west and the Elwha River delta to the east. Coville Creek and the Pliocene-Oligocene marine sedimentary outcrop are in center of Freshwater Bay.

Figure 3

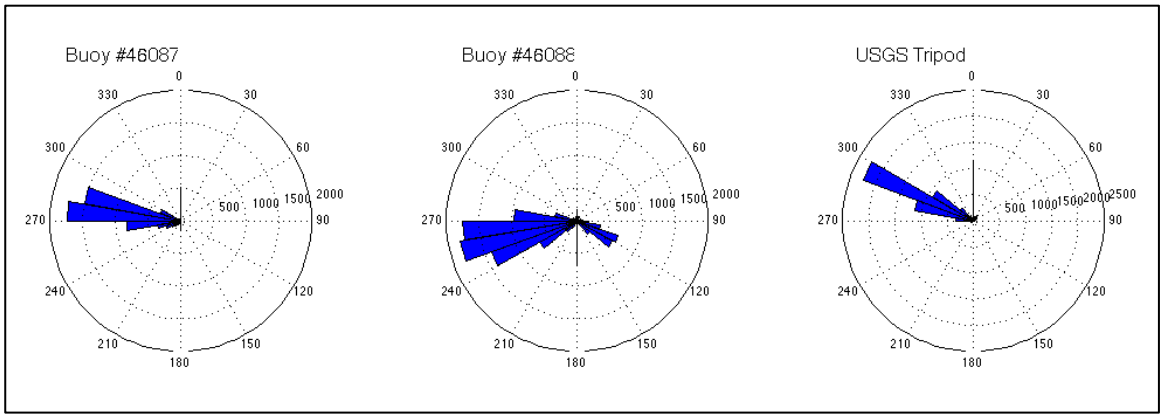

Figure 3a. Comparison of dominant wave energy direction at a USGS instrument tripod and at two NDBC buoys; Neah Bay (#46087) and New Dungeness (#46088). Radial axes are frequency of event; NDBC buoys maximum scale is 2000, USGS tripod maximum scale is 2500. USGS tripod only measures from 270°-90° since both southern quadrants are blocked by the landmass of the Olympic Peninsula. Secondary mode for Buoy #46088 at 120° indicates southerlies exiting the Puget Sound main basin. (USGS data courtesy of Jon Warrick)

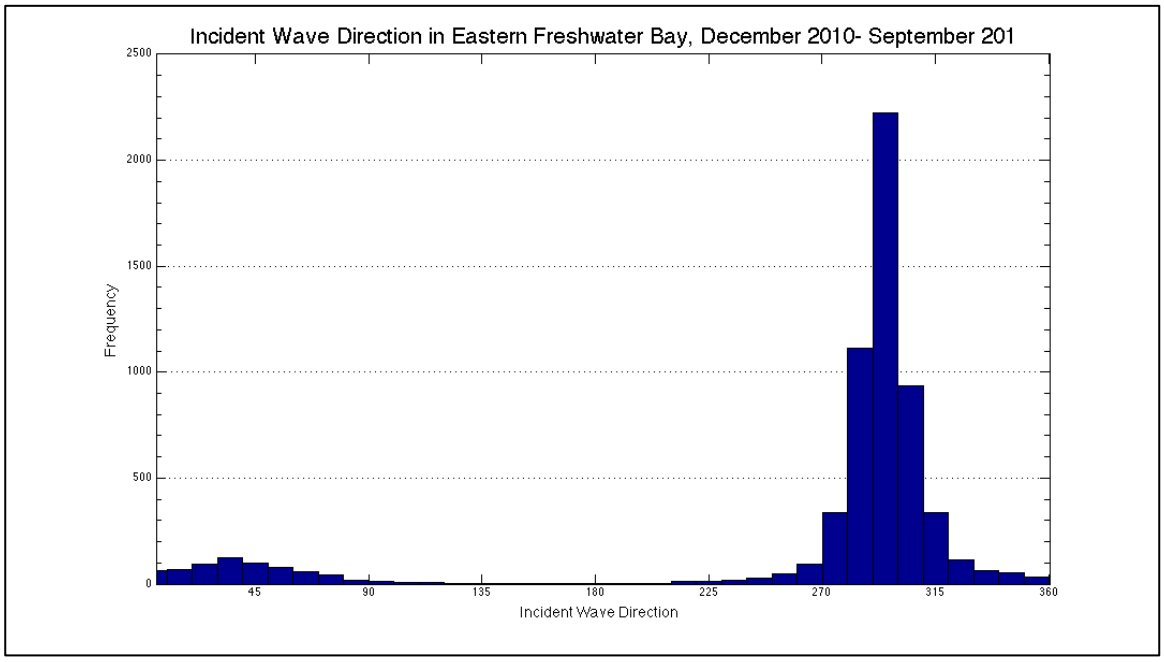

Figure 3b. Histogram showing the dominant wave period incident direction at the USGS instrument tripod in eastern Freshwater Bay, Washington, USA. Notice the bins 0-90 showing NE waves for 10% of the data acquisition period. This fraction is not discernible in Figure 3a. (USGS data courtesy of Jon Warrick)

Figure 4

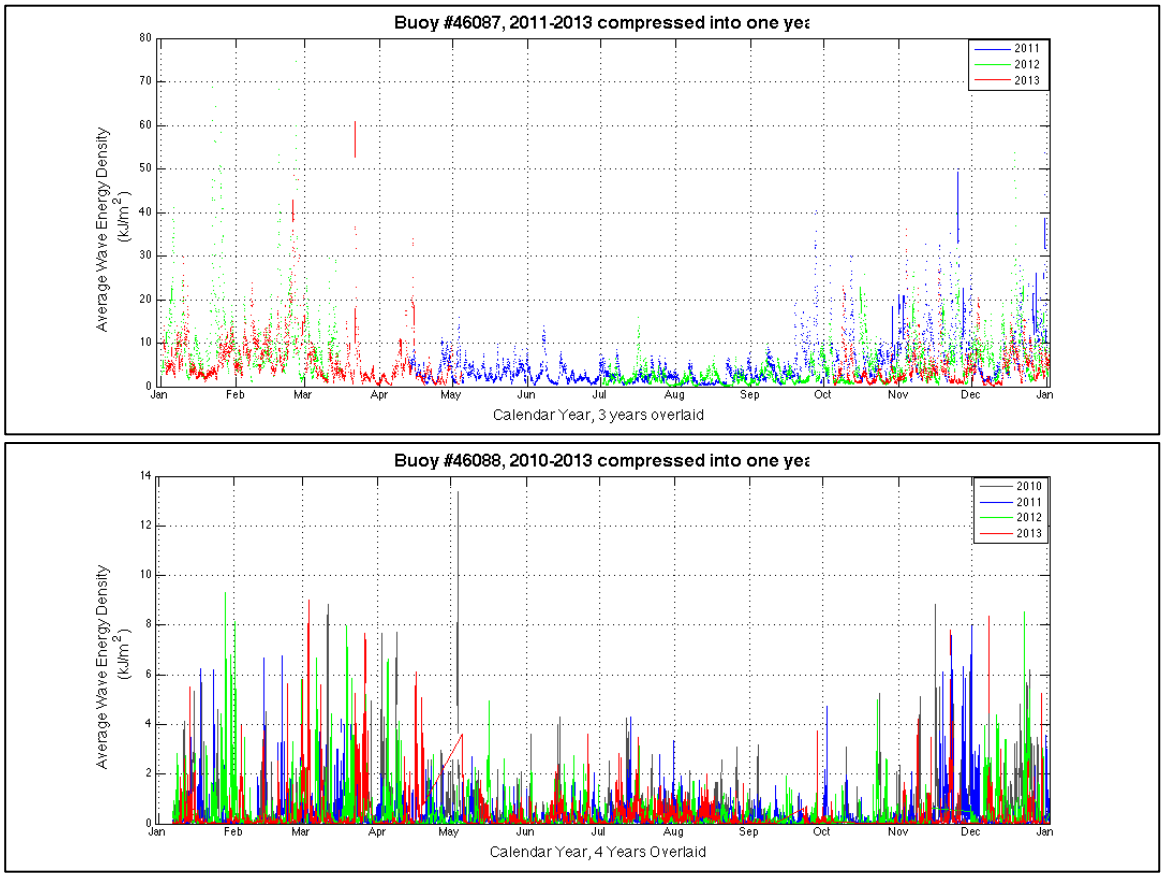

Figure 4. Wave energy density in kJm^{-2}. Top panel of Neah Bay (Buoy #46087) shows large gaps when no data were available. Wave energy density is reduced between May and mid-Sept., but note that some months only record data from a single year. Lower panel is New Dungeness (Buoy #46088) and shows nearly complete record of data from a four-year period. This compilation again shows reduced wave energy density between May and mid-Sept. Note the reduced scale at New Dungeness of a maximum (early May) of 14 kJm^{-2} versus a maximum at Neah Bay of 60 kJm^{-2} in late March.

Figure 5

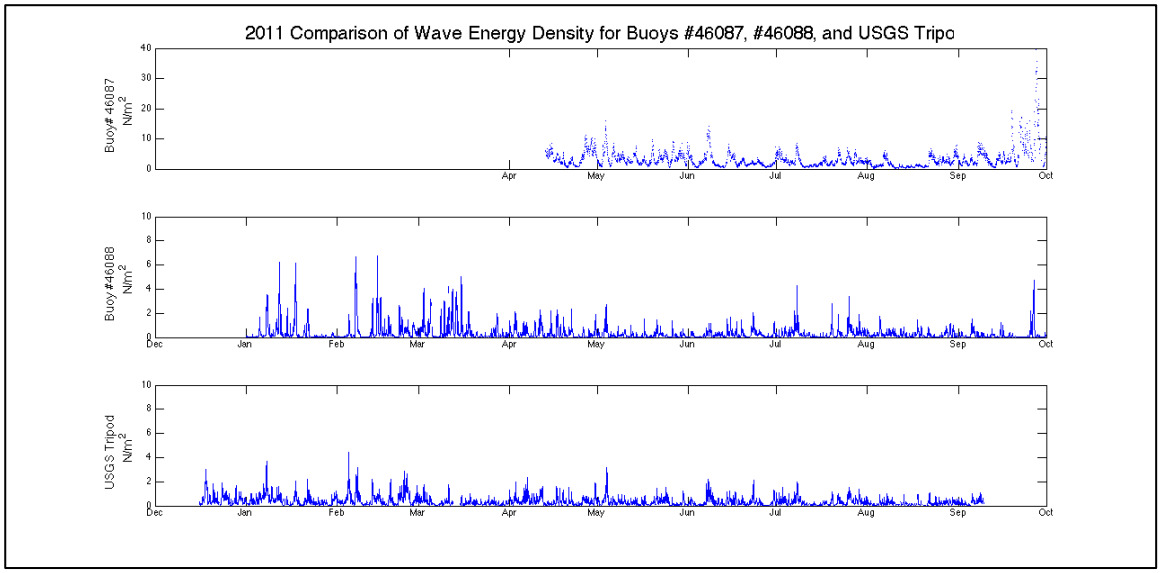

Figure 5. Comparison of wave energy density in kJm^{-2} for the first three quarters of 2011. Top panel is Neah Bay (Buoy #46087), middle panel is New Dungeness (Buoy #46088) and lower panel is USGS instrument tripod located in the Elwha delta nearshore environment in ~10m water depth. (USGS data courtesy of Jon Warrick)

Figure 6

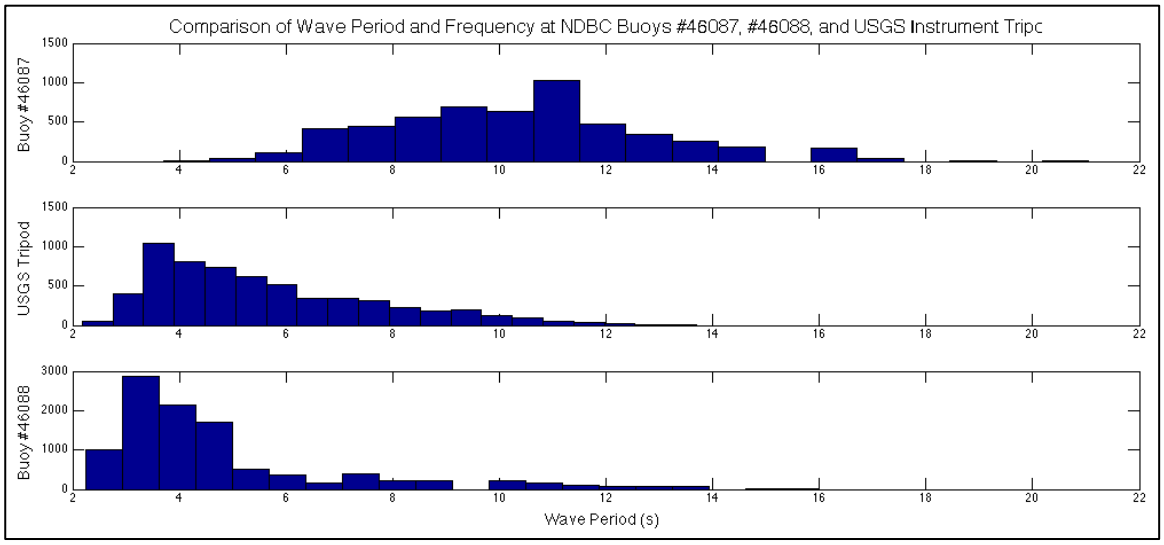

Figure 6. Frequency histogram for NDBC buoys and USGS instrument tripod. Neah Bay (Buoy #46087) has longer mean wave period with a normal distribution. New Dungeness (Buoy #46088) and the USGS tripod on the Elwha delta have a right-tailed distribution and a shorter mean wave period. Horizontal scales are identical, but notice Buoy #46088 has a higher frequency of occurrence for the mode. (USGS data courtesy of Jon Warrick)

Figure 7

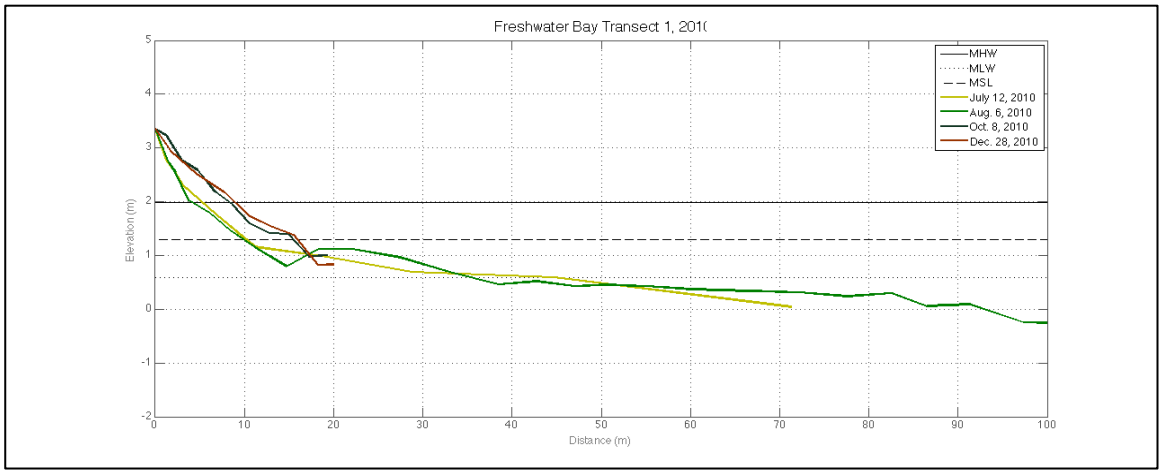

Figure 7a.

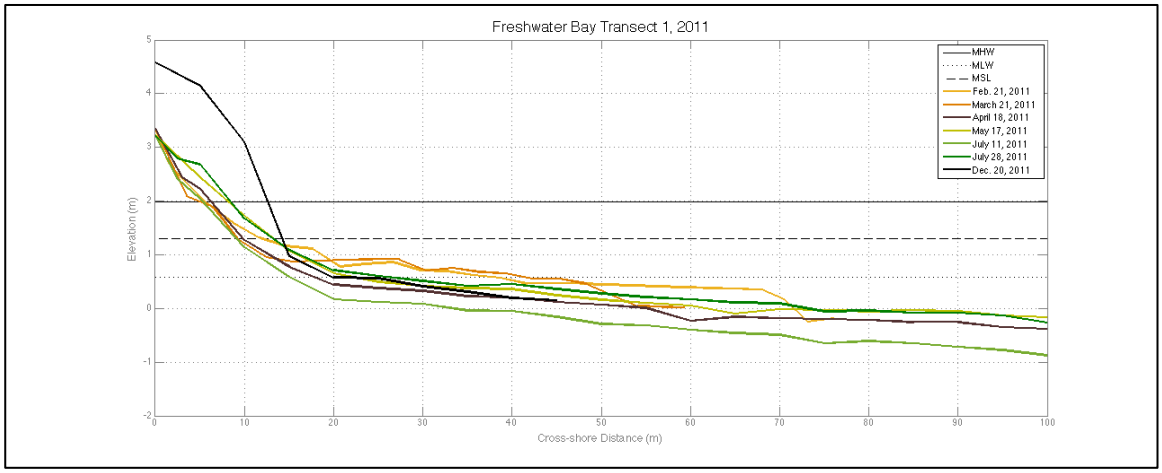

Figure 7b.

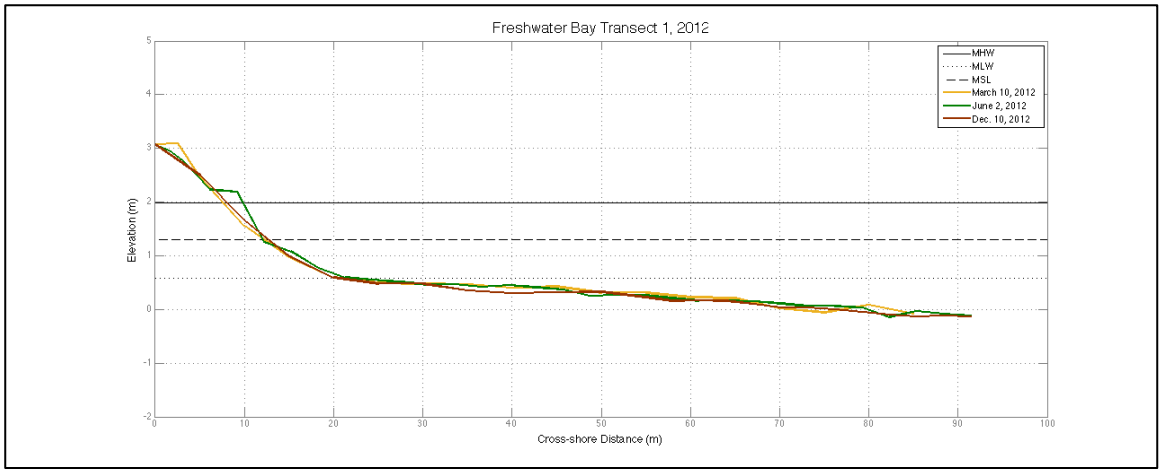

Figure 7c.

Continued on next page.

Figure 7, cont.

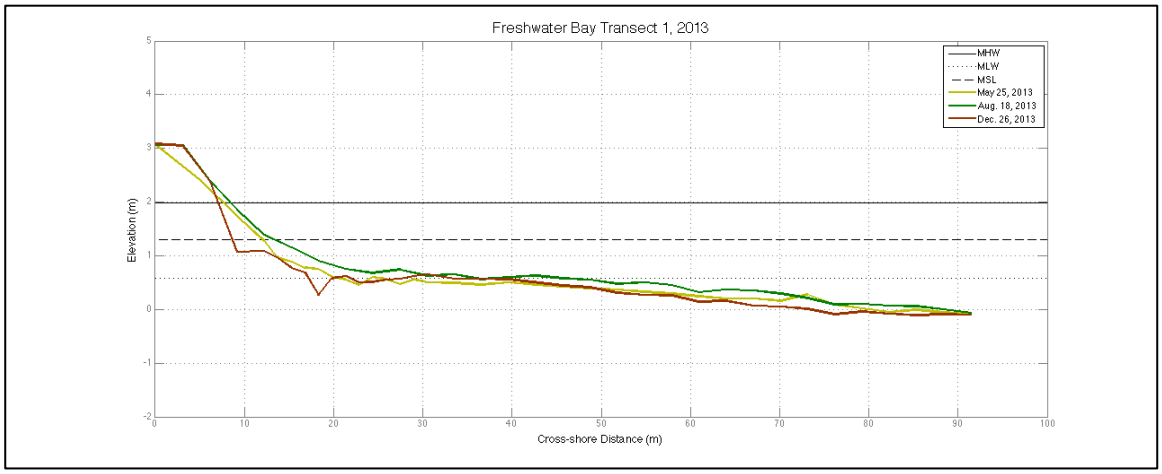

Figure 7d.

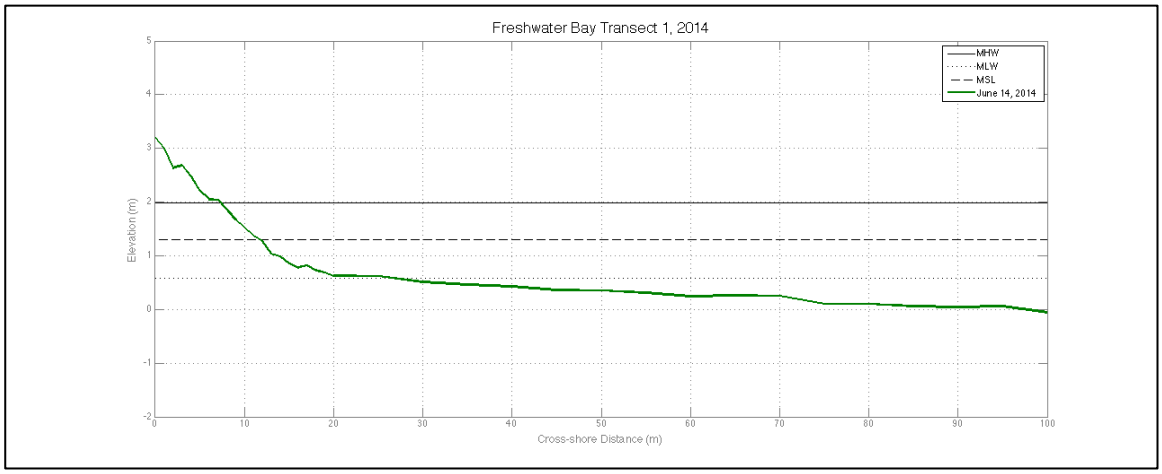

Figure 7e.

Figure 7. Five panels showing Transect 1 in western Freshwater Bay from 2010-2014, see Figure 2 for location. Profiles with green colors indicate low-energy wave environment from mid-May through Sept. Brown profiles indicate high-energy environment from Oct. through Mid-May. Identical vertical and horizontal scales are used for each panel. Mean High Water (MHW), Mean Sea Level (MSL), and Mean Low Water (MLW), origin at MLLW with North American Vertical Datum 1988 (NAVD88). Vertical exaggeration is 6.25:1. (All profile data courtesy of Dave Parks, Wash. DNR)

Figure 8

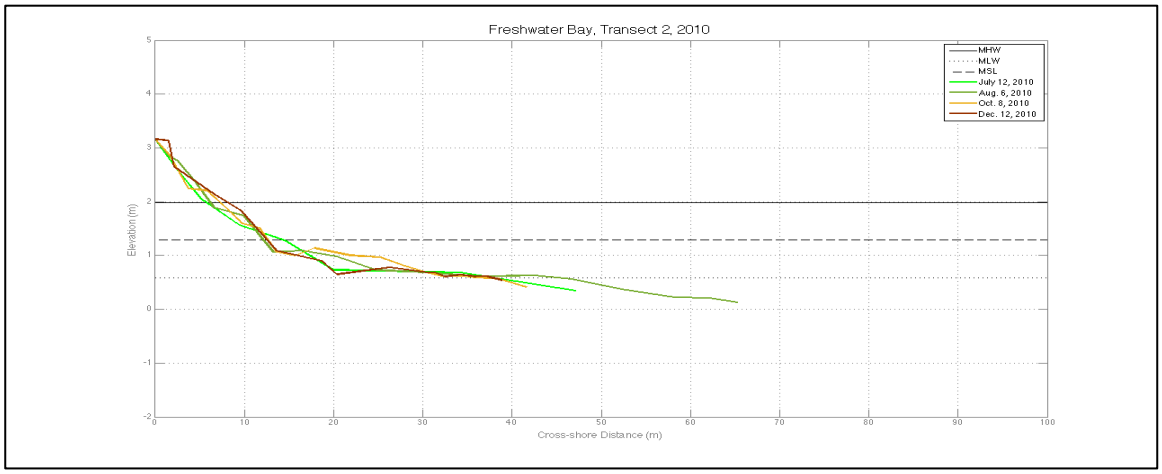

Figure 8a.

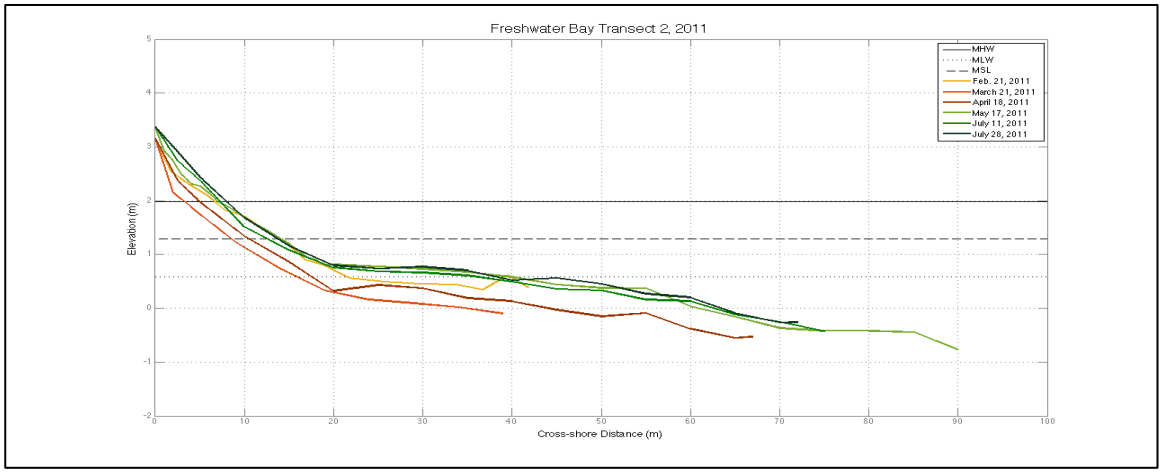

Figure 8b.

Continued on next page.

Figure 8, cont.

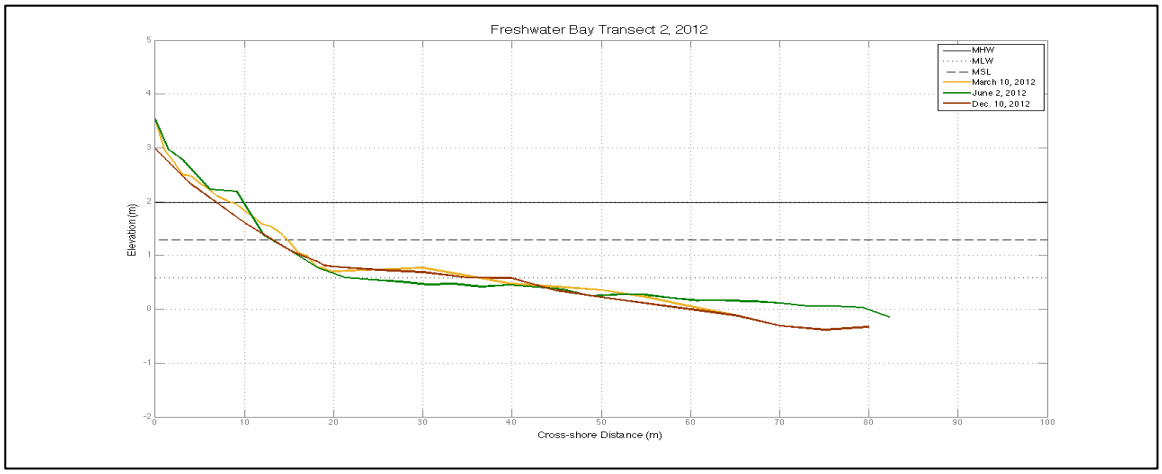

Figure 8c.

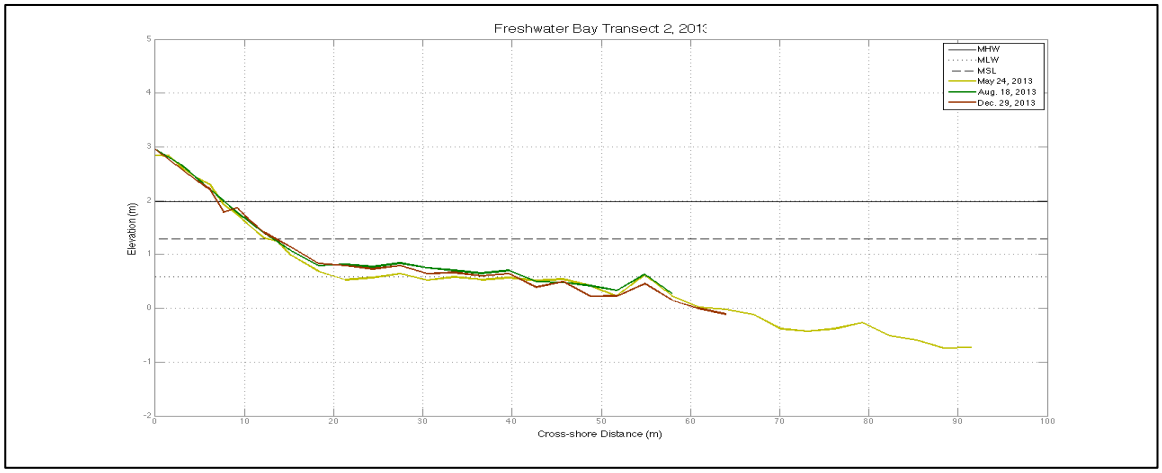

Figure 8d.

Figure 8. Four panels showing Transect 2 in western Freshwater Bay from 2010-2013, see Figure 2 for location. Note that no profiles were collected in 2014. Profiles with green colors indicate low-energy wave environment from mid-May through Sept. Brown profiles indicate high-energy environment from Oct. through Mid-May. Identical vertical and horizontal scales are used for each panel. Mean High Water (MHW), Mean Sea Level (MSL), and Mean Low Water (MLW), origin at MLLW with North American Vertical Datum 1988 (NAVD88). Vertical exaggeration is 6.25:1. (All profile data courtesy of Dave Parks, Wash. DNR)

Figure 9

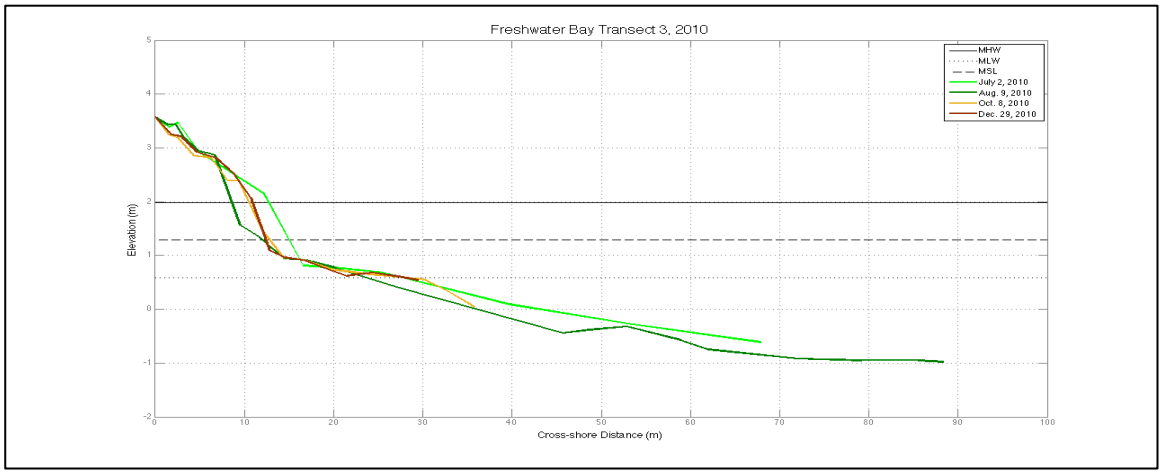

Figure 9a.

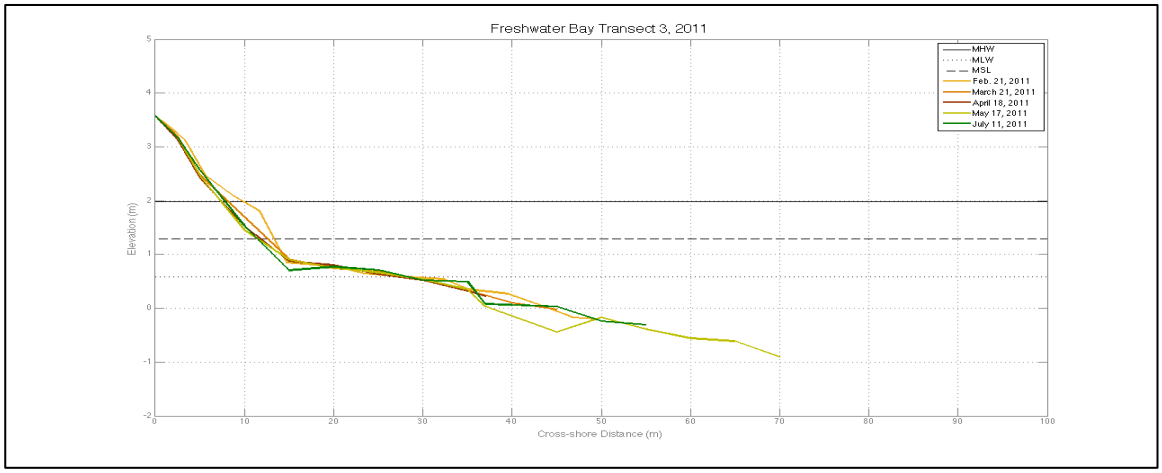

Figure 9b.

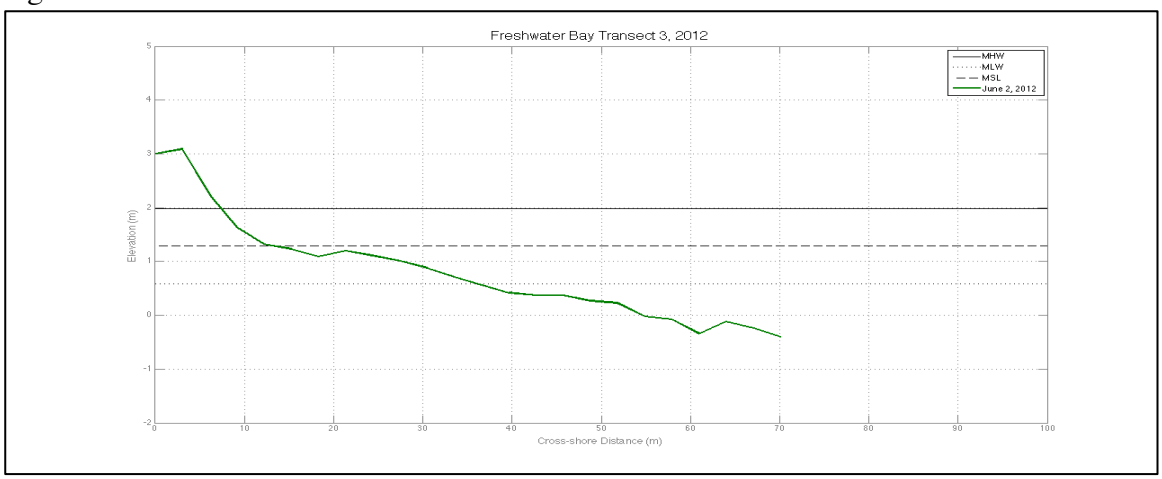

Figure 9c.

Continued on next page.

Figure 9, cont.

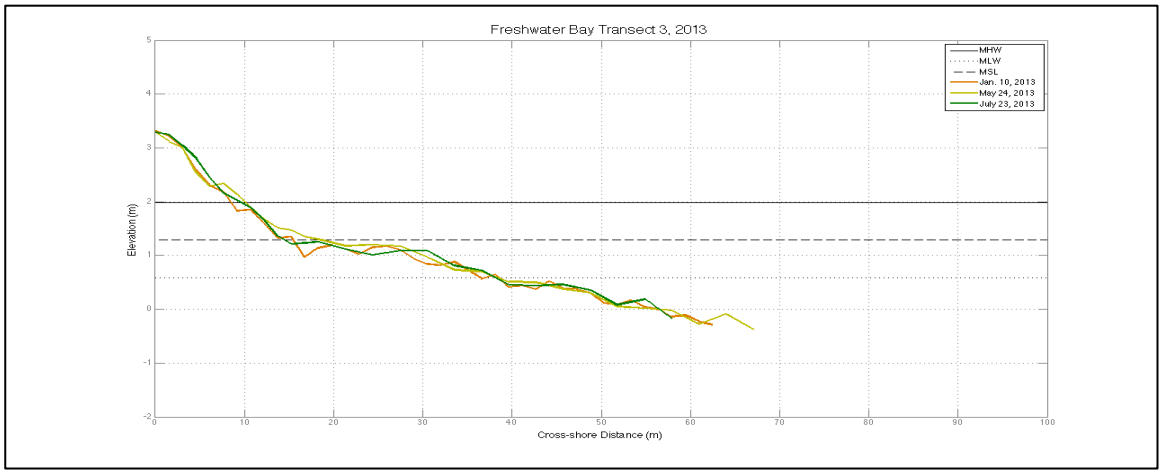

Figure 9d.

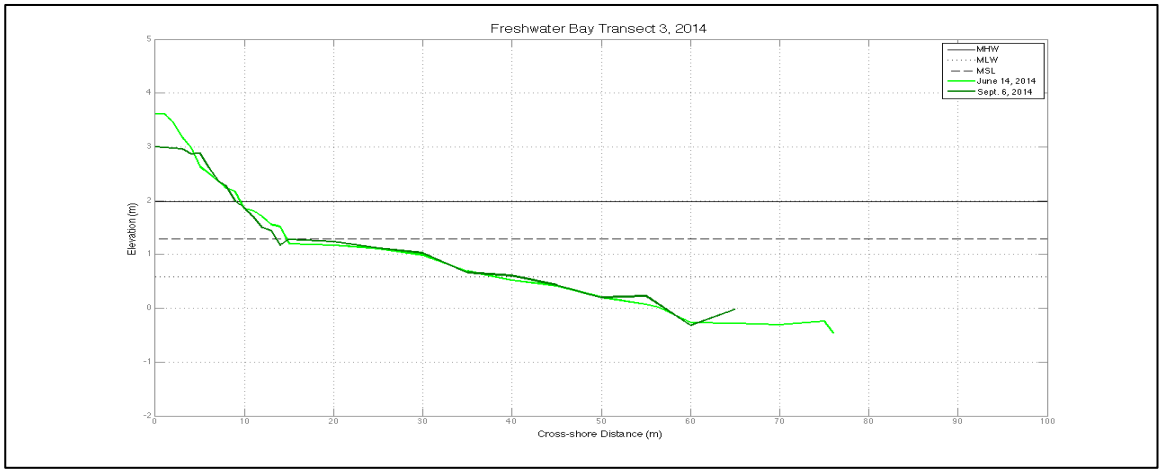

Figure 9e.

Figure 9. Five panels showing Transect 3 in eastern Freshwater Bay from 2010-2014, see Figure 2 for location. Profiles with green colors indicate low-energy wave environment from mid-May through Sept. Brown profiles indicate high-energy environment from Oct. through Mid-May. Identical vertical and horizontal scales are used for each panel. Mean High Water (MHW), Mean Sea Level (MSL), and Mean Low Water (MLW), origin at MLLW with North American Vertical Datum 1988 (NAVD88). Vertical exaggeration is 6.25:1. (All profile data courtesy of Dave Parks, Wash. DNR)

Figure 10

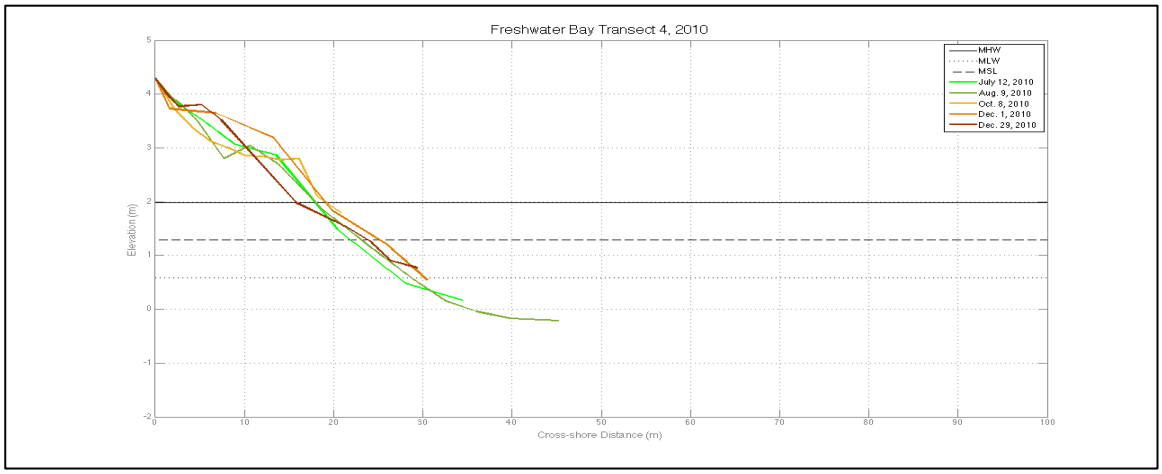

Figure 10a.

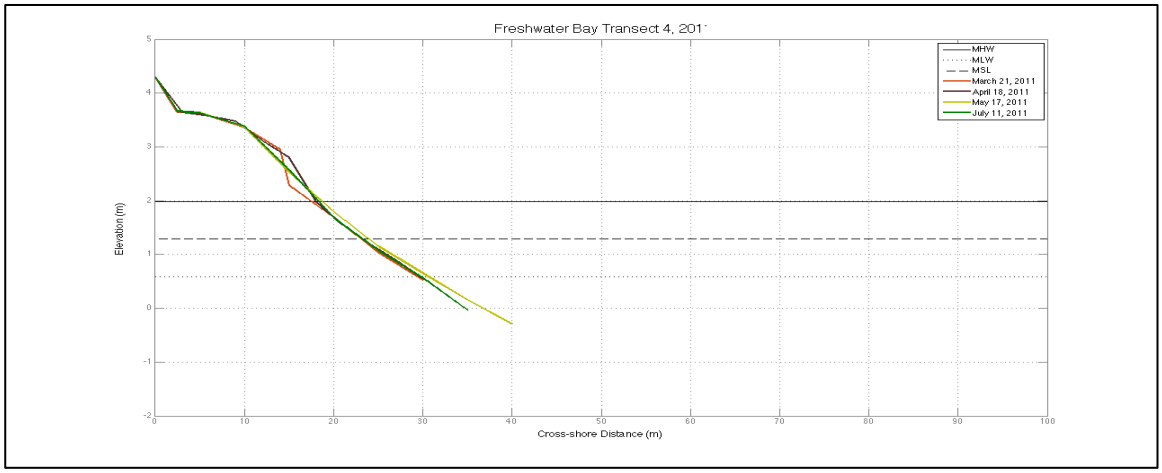

Figure 10b.

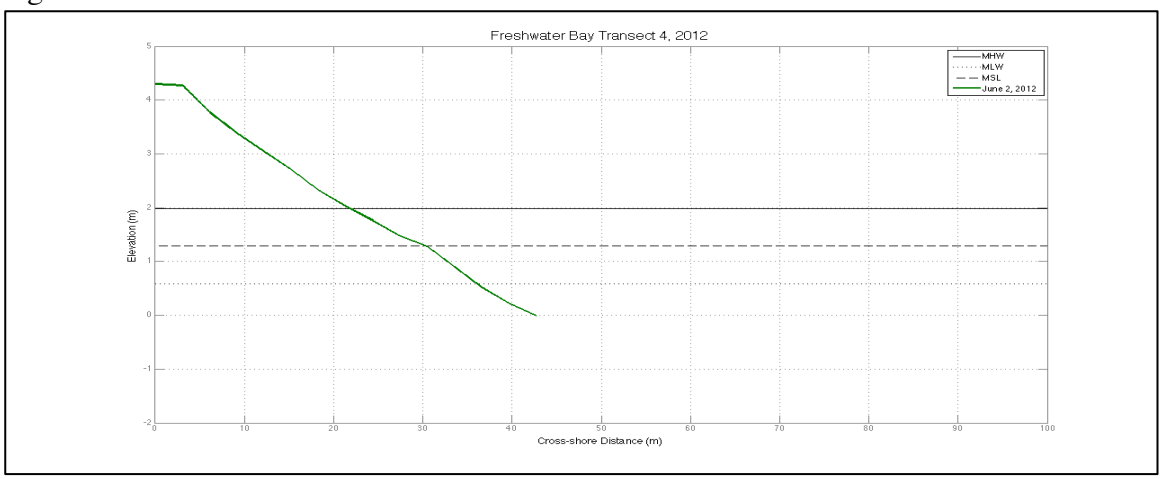

Figure 10c.

Continued on next page.

Figure 10, cont.

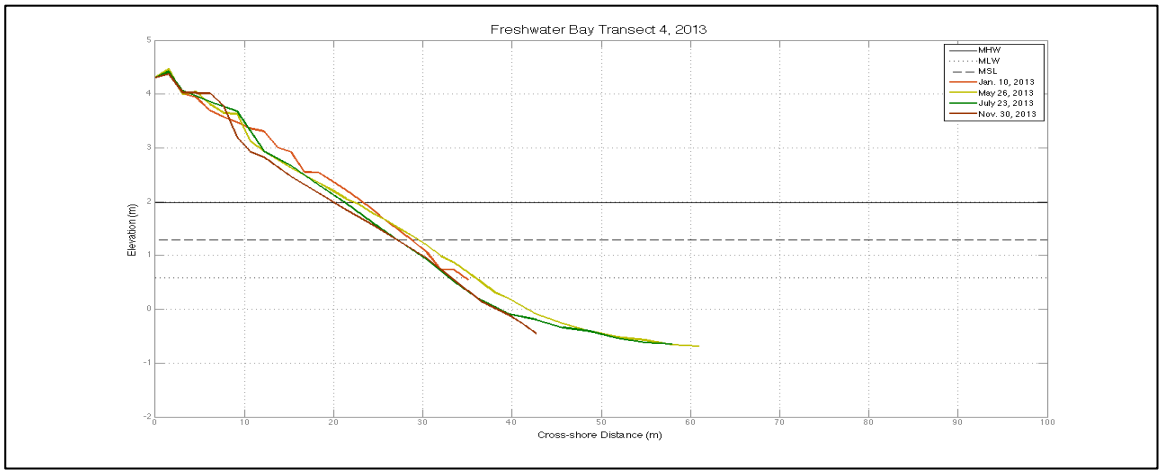

Figure 10d.

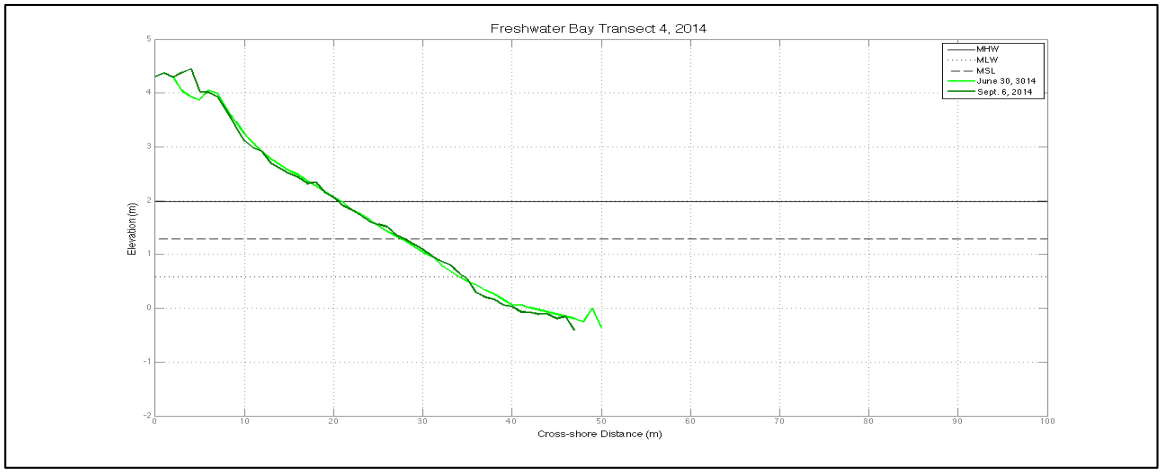

Figure 10e.

Figure 10. Five panels showing Transect 4 in eastern Freshwater Bay from 2010-2014, see Figure 2 for location. Profiles with green colors indicate low-energy wave environment from mid-May through Sept. Brown profiles indicate high-energy environment from Oct. through Mid-May. Identical vertical and horizontal scales are used for each panel. Mean High Water (MHW), Mean Sea Level (MSL), and Mean Low Water (MLW), origin at MLLW with North American Vertical Datum 1988 (NAVD88). Vertical exaggeration is 6.25:1. (All profile data courtesy of Dave Parks, Wash. DNR)

Figure 11

A B

Figure 11. Slope break sediment grain size images for Transect 1 at ~20 m cross-shore for Aug. 18, 2013 (A) and Dec. 29, 2013 (B). Both images are categorized as predominantly cobble with gravel but image B has experienced an elevation decrease of 0.64 m. A plunge point and seaward ridge formed at the location of B. This is evidence of large grains moving in relatively short periods of time. (Images courtesy of Dave Parks, Wash. DNR)

Figure 12

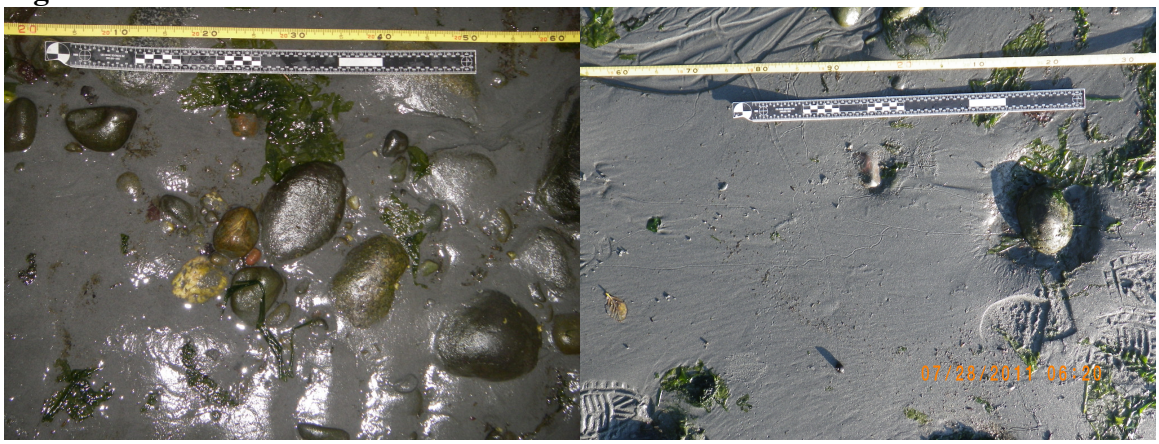

A B

Figure 12. Slope break sediment grain size images for Transect 1 at ~20 m cross-shore for July 11, 2011 (A) and July 28, 2011 (B). Both images are categorized as sand-with-fines. Image B is after an elevation increase of ~0.50 m. Increased elevation occurred along the entire transect to 100 m cross-shore. Image B has surface sediment of primarily sand-with-fines but gravel and cobble are also present. This is evidence of large volumes of sediment with some larger particles moving in very short time periods. (Images courtesy of Dave Parks, Wash. DNR)

Figure 13

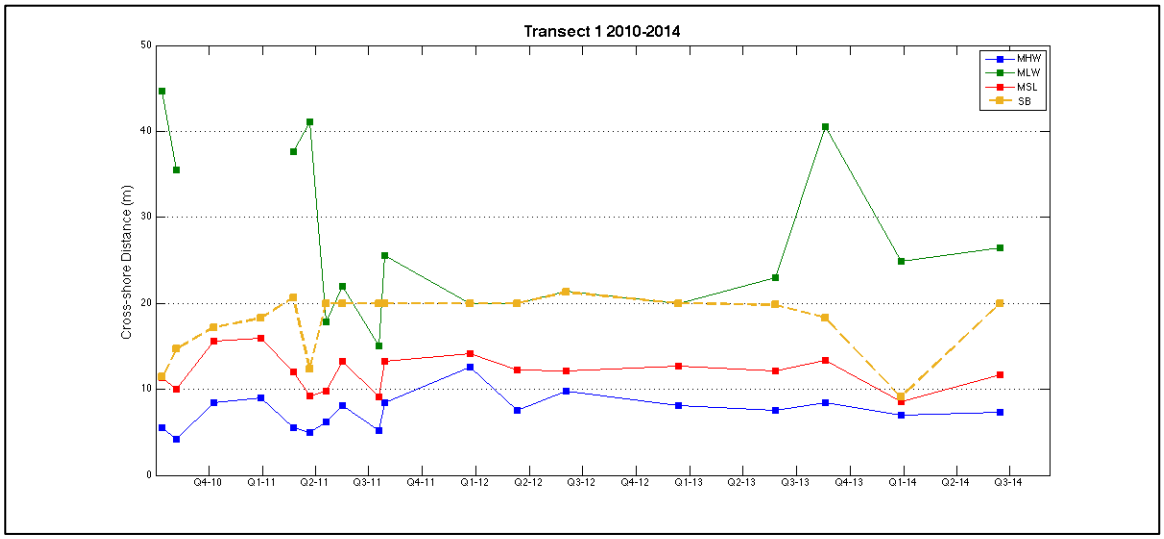

Figure 13. Transect 1 in western Freshwater Bay (FWB), nearest Observatory Point. Horizontal axis is timescale from third quarter 2010 through third quarter 2014. Mean High water (MHW) is 1.987m, Mean Sea Level (MSL) is 1.295m, Mean Low Water (MLW) is 0.586m above North American Vertical Datum of 1988 (NAV88). SB varies in cross-shore position and elevation through time. Notice erosional events in Q2-11, Q3-11, and Q1-14. Extension of low-tide terrace in Q1-11 and Q3-13 indicate deposition. (All profile data courtesy of Dave Parks, Wash. DNR)

Figure 14

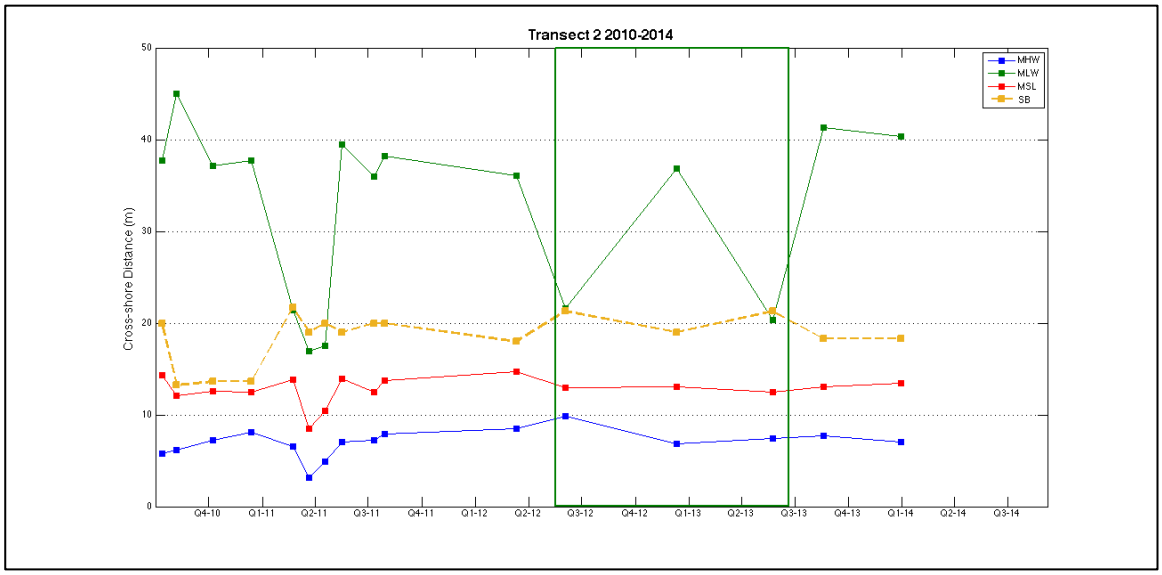

Figure 14. Transect 2 in FWB, moving east of Transect 1, but still in western FWB. This transect also has an erosional event in Q2-11 and apparent cyclic deposition and removal of sediment from the low-tide terrace, see Q2-11, Q2-12, and Q2-13 for removal portion of this cycle. Green box shows a one-year period with MHW regression accompanied by deposition on the low-tide delta between MLW and SB. (All profile data courtesy of Dave Parks, Wash. DNR)

Figure 15

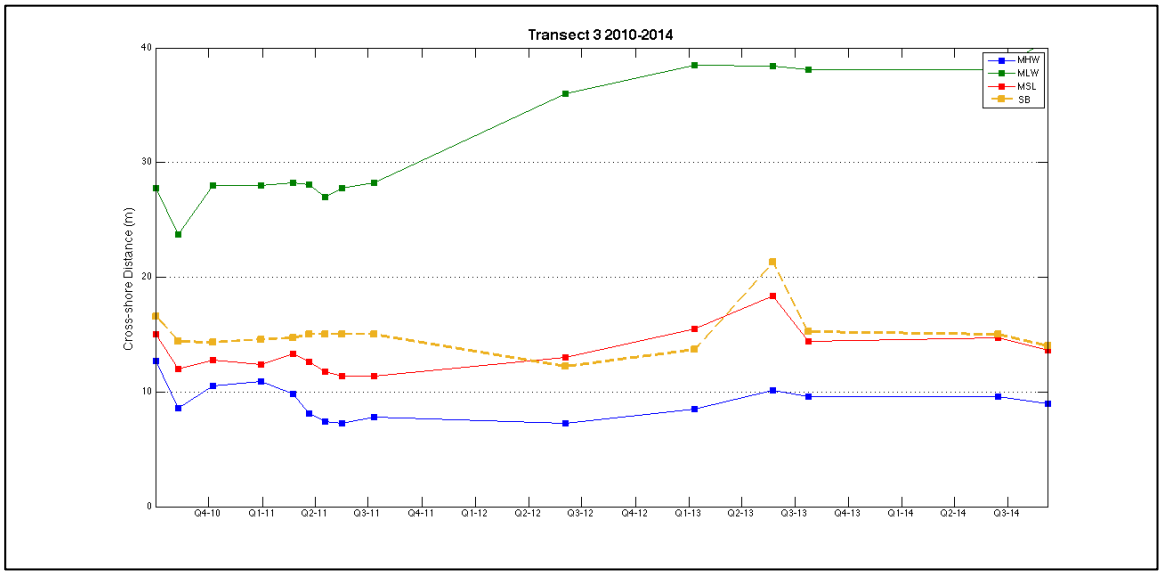

Figure 15. Transect 3 in eastern Freshwater Bay. Notice long-term trend to deposition at MHW and MSL. From Q3-11 onward there is substantial increase of MLW cross-shore position indicating long-term deposition on the low-tide terrace. Also visible is a seaward movement of MSL and MHW, indicating deposition on the shoreface above the SB. (All profile data courtesy of Dave Parks, Wash. DNR)

Figure 16

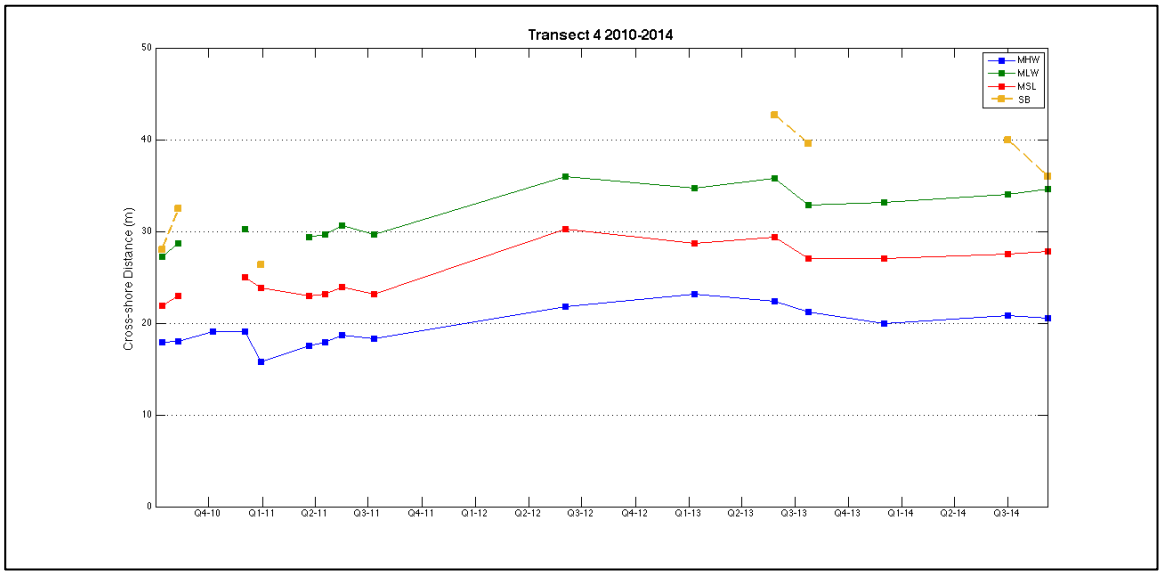

Figure 16. Transect 4 has minimal data showing SB. Long-term trend is beach-face extension seaward at MHW, MSL, and MLW, with most noticeable event from Q2-12 through Q2-13. This is possibly an expression of increased sediment supply from the Elwha River. (All profile data courtesy of Dave Parks, Wash. DNR)

Tables

Table 1. Mean wave period for dominant waves at Elwha River delta USGS instrument tripod and NDBC Buoy's #46088 and #46087 for mid-Dec. 2010 through Sept. 2011. Wavelength derived from Airy Wave Theory. USGS tripod wavelengths given are for shallow water (depth/wavelength < 1/20) and deep water (depth/wavelength > 1/4) derivations, intermediate water conditions will fall between these lengths. Wave height is significant wave height (highest 1/3 of waves recorded) at buoy or instrument tripod.

Location (units) [water depth]	mean	min.	max.	range	wave length
Tripod period (s) [9.78 m]	5.6	2.2	13.7	11.5	54.8 m (shallow)
Tripod wave height (m)	0	0.05	1.87	1.82	49 m (deep)
Buoy #46088 period(s)[118.9 m]	4.8	2.2	16	13.7	36 m (deep)
Buoy #46088 wave height (m)	0.4	0.04	2.5	2.47	
Buoy #46087 period(s)[256.6 m]	10.3	3.7	21	17.3	165.6 m (deep)
Buoy #46087 wave height (m)	1.7	0.4	6.5	6.1	
Wave energy density of dominant period waves (kJ/m^2)	mean	min.	max.	range	
Buoy #46087 (Neah Bay)	3.66	2.02	53.5	51.5	
Buoy #46088 (New Dungeness)	2.02	0.002	7.91	7.91	
USGS tripod (Elwha delta)	2.92	0.003	4.43	4.43	
Wave energy density compared to Neah Bay (percent)	mean	min.	max.	range	
Buoy #46087	100%	100%	100%	100%	
Buoy #46088	55%	0.10%	14.8%	15.4%	
USGS tripod	80%	0.14%	8.3%	8.6%	

Table 2. Bed surface sediment grain-size at the slope break and Mean Low Water for four transect locations in FWB (T1-T4). Table uses a visual scale: 1= sand-with-fines, 2 = sand, 3 = gravel, 4 = cobble. When two adjacent size classes have approximately equal representation in the image, then a fractional value midway between the size classes is used, i.e. ~50% gravel (3) and ~50% cobble (4) in one image results in a 3.5 for that image. If two non-adjacent size classes are equally represented, the intervening size class is not used, i.e. ~50% sand (2) and ~50% cobble (4) are not represented by a (3) in the table. In this case the larger size classification is used. Open boxes indicate unusable images. (data courtesy of Dave Parks, Wash. DNR)

Slope Break					**Mean Low Water**				
DATE:	T 1	T 2	T 3	T 4	**DATE:**	T 1	T 2	T 3	T 4
7/2/10			3.5		7/2/10			3.5	
7/12/10	3	1		2.5	7/12/10	2.5	1		2
8/6/10	3	2			8/6/10		4		
8/9/10					8/9/10				
10/8/10		4	4		10/8/10			4	
12/1/10					12/1/10				
12/12/10		2			12/12/10		4		
12/28/10	3.5								
12/29/10			2.5	2	12/29/10				
2/21/11	2	3	3		2/21/11		4	3.5	
3/21/11	2	2.5	3		3/21/11	2.5	2.5	3.5	2.5
4/18/11	1	2.5	3.5		4/18/11	2	2.5	4	2
5/17/11	1	2	3.5		5/17/11	2	4	3.5	2
7/11/11		3	3.5		7/11/11	2	4	3.5	2
7/17/11	1								
7/28/11	1	4			7/28/11		4		
12/20/11									
3/10/12		4			3/10/12		3.5		
6/2/12		2			6/2/12		2		
12/10/12		3			12/10/12		3.5		
1/10/13			4		1/10/13	2		2	2
5/24/13		4	3.5		5/24/13		3.5	3.5	
5/25/13	4								
5/26/13				1	5/26/13	2			2
7/23/13			3.5	1	7/23/13	2		3.5	2
8/18/13	4	3			8/18/13		4		
11/30/13					11/30/13	2			2
12/26/13	3								
12/29/13		4			12/29/13		4		
6/14/14	3.5		3.5		6/14/14			3.5	
6/30/14				1	6/30/14	2			2
9/6/14			3.5	2	9/6/14	3		3.5	3

Table 3. Bed surface sediment grain-size at Mean High Water and Mean Sea Level for four transect locations in FWB (T1-T4). Table uses a visual scale: 1= sand-with-fines, 2 = sand, 3 = gravel, 4 = cobble. When two adjacent size classes have approximately equal representation in the image, then a fractional value midway between the size classes is used, i.e. ~50% gravel (3) and ~50% cobble (4) in one image results in a 3.5 for that image. If two non-adjacent size classes are equally represented, the intervening size class is not used, i.e. ~50% sand (2) and ~50% cobble (4) are not represented by a (3) in the table. In this case the larger size classification is used. Open boxes indicate unusable images. (data courtesy of Dave Parks, Wash. DNR)

Mean High Water

DATE:	T 1	T 2	T 3	T 4
7/2/2010			2	
7/12/10	3	3		2
8/6/10	3	3		
8/9/10				
10/8/10	3	3	3	3
12/1/10				
12/12/10		2		
12/28/10	2.5			
12/29/10			2	2
2/21/11	3	2	2	
3/21/11	2	2	2	2
4/18/11	3	2	3	
5/17/11	3	2.5	3	2
7/11/11		2.5	2	3
7/17/11	3			
7/28/11	3	3		
12/20/11				
3/10/12		2		
3/10/12				
6/2/12				
12/10/12		2		
1/10/13			2.5	2
5/24/13		2.5	2.5	
5/25/13	3			
5/26/13				2
7/23/13			2	2
8/18/13	2.5	3		
11/30/13				2
12/26/13	3			
12/29/13		2		
6/14/14	2.5		2	
6/30/14				2
9/6/14			3	2

Mean Sea Level

DATE:	T 1	T 2	T 3	T 4
7/2/10			3	
7/12/10	3	2		2
8/6/10	2.5	2		
8/9/10				
10/8/10		4	4	
12/1/10				
12/12/10		2		
12/28/10	3.5			
12/29/10			2	2
2/21/11	3	2	3	
3/21/11	2	2	3	2
4/18/11	2.5	2	3.5	2
5/17/11	1	2	3.5	2
7/17/11	3	3.5	2.5	2.5
7/28/11	2	2.5		
12/20/11				
3/10/12		3		
6/2/12				
12/10/12		2.5		
1/10/13			3.5	2
5/24/13		2	3.5	
5/25/13	3			
5/26/13				2
7/23/13			2.5	2
8/18/13	3	3		
11/30/13				2
12/26/13	3			
12/29/13		2.5		
6/14/14	2.5		3.5	
6/30/14				2
9/6/14			3.5	2